Emerging Two–Dimensional Intercalation Pseudocapacitive Electrodes for Supercapacitors

Sarojini Jeeva Panchu,[a] Kumar Raju,*[b] and Hendrik C. Swart*[a]

The growing need for efficient energy storage has spurred advancements in supercapacitors (SCs), aiming to offer high power and energy density simultaneously. While SCs offer longer cycles and higher power density values, their low energy densities limit practical applications. In response, pseudocapacitive materials have emerged, leveraging reversible Faradaic reactions at or near the surface for enhanced energy storage. This approach surpasses the constraints of the electrical double layer in SCs and the mass transfer constraints of batteries. Progress in asymmetric supercapacitors and high mass loading has improved energy density values, yet maintaining high mass loading without compromising power density remains a hurdle. Advancements in pseudocapacitance through intercalation during charging/discharging processes, especially in layered structures like graphite, graphene, transition metal oxides (TMOs) transition metal dichalcogenides (TMDCs), MXenes, and metal–organic frameworks (MOFs) have proven significant. The intercalated species induce reversible or irreversible structural changes, contributing to the physicochemical characteristics of the electrode materials. Exploring the intercalation mechanism in bulk two-dimensional (2D) materials reveals distinct differences that enhance our understanding and improve electrochemical properties for superior energy storage. Finally, an in-depth exploration of the intercalation pseudocapacitance in 2D materials such as TMDCs and MXenes underscores their significance, setting a benchmark for future electrochemical studies in the subsequent advancement of SCs research.

1. Introduction

The variability of renewable energies has led to an increased need for advanced energy storage solutions to effectively capture and utilize electricity generated from renewable sources. Among the array of energy storage technologies, batteries, and supercapacitors (SCs) stand out as leading electrochemical energy storage devices, characterized by their notable specific energy and power densities.[1–3] Besides the growth of SCs has rapidly accelerated in response to increasing energy storage needs and addressing environmental challenges.[4,5]

With the surge in consumer electronics, SCs have gained popularity after being developed as forms of energy storage devices, features such as high–power density, safety, higher performance with long term stability over Lithium-ion batteries. Unlike standard dielectric capacitors, supercapacitors offer greater power density and longer cycle life than batteries.[6,7] SCs developed with high energy density values serve as substitutes in many battery–powered electronics. However, the current generation's performance falls short of the demands of wearable electronics, hybrid electric vehicles, and large systems that require high energy and power densities. SCs store energy through electric double layers or Faradaic reactions, such as surface redox reactions and ion intercalation, termed pseudocapacitive due to their fast redox reaction on the surface.[8] The intercalation pseudocapacitance happens when ions insert into the layers of redox–active materials, causing a charge transfer along with faradaic charge transfer.[9] Unlike in lithium–ion batteries where this often involves a phase change in the material, in pseudocapacitance, no such change occurs. The link between electric double layer capacitors (EDLCs) and batteries can be bridged by materials with pseudocapacitive characteristics. However, Inherently, their slow ion transfer rates make them unsuitable for successful commercialization because of their poor electrical conductivity as well as cyclability.[10] As a result of the limitations of traditional electrodes, significant research interests are being directed towards the development of electrode materials exhibiting outstanding electrochemical performance to achieve high–energy density electrodes. Recent advancements in nanostructured materials, with much smaller particle sizes than diffusion lengths or redox–active functionalized carbons, blur the boundaries. Pseudocapacitive materials exhibit highly reversible electrochemical responses, independent of solid–state diffusion, making them highly efficient.

Choosing the right electrode material is crucial for optimizing the electrochemical characteristics of SCs. Several 2D materials and their nanocomposites are being investigated for their potential use for SCs as an electrodes based on their unique electrochemical features. An understanding of the surface structure of 2D nanomaterials is crucial when investigating these materials' bulk electrochemical properties owing to

[a] S. J. Panchu, Prof. H. C. Swart
Department of Physics, University of the Free State, Bloemfontein-9301, South Africa
E-mail: swarthc@ufs.ac.za
[b] K. Raju
Institute for Manufacturing, University of Cambridge, Cambridge, CB3 0FS, UK
E-mail: kr516@cam.ac.uk

© 2024 The Authors. ChemElectroChem published by Wiley-VCH GmbH. This is an open access article under the terms of the Creative Commons Attribution License, which permits use, distribution and reproduction in any medium, provided the original work is properly cited.

the fact that their atoms reside at their surfaces. The intrinsic surface on 2D nanomaterials possesses characteristics in controlling the surface charges for the charge storage techniques for the SCs leading to enabling the development of capacitive materials through chemical surface treatments and hybrid architectures for the development of high energy/power SCs.[11] With appropriate surface chemistry and multidimensional design, 2D nanomaterials enhance ion and electron diffusion rates as well as storage capabilities.[12] Pseudocapacitors are capable of expanding SC rate capabilities and energy

Sarojini Jeeva Panchu is a Post–Doctoral Researcher in Prof Hendrik C Swart research group in the Department of Physics, University of the Free State, Bloemfontein campus. She completed her Doctoral degree in Physics at University of KwaZulu–Natal, Durban, South Africa in 2020. She was awarded a National Research Foundation (NRF) freestanding Doctoral scholarship. She was working as a research assistant in CSIR-Central Electrochemical Research Institute in India (2012–2016). She completed her Master degree in Physics at Madurai Kamaraj University in India (2012). Her current research project on the topic of development of two-dimensional nanostructured materials for energy storage and energy conversion devices.

Kumar Raju is currently a Faraday Institution Research Fellow at the Institute of Manufacturing (IfM), Department of Engineering, University of Cambridge, United Kingdom. His academic journey commenced with his doctoral research at the University of Madras, followed by postdoctoral work at Hanyang University, South Korea, and subsequent tenure as a Senior Research Scientist at the Energy Centre, Council for Scientific and Industrial Research (CSIR), South Africa. His current research involves the processing of advanced electrode materials, including the development of novel methods to structure electrode materials and to study their processing into advanced electrodes for lithium-ion batteries and supercapacitors.

Prof. Hendrik C. Swart is a B1 NRF rated researcher (Internationally acclaimed researchers) and currently a senior professor in the Department of Physics at the University of the Free State. He brought luminescence materials to South Africa in the beginning of 1996 after a highly productive sabbatical spend in the lab of Paul Holloway, Florida University, Gainesville. This laid the foundation for his subsequent research at the UFS and was one of the most exhilarating times of his academic career. Since than he has led research in the area of the degradation of phosphors for field emission displays, as well as developing materials for nano solid-state lighting. He has been key in the development of processes to synthesise and deposit thin films of various types of semiconductor nano-particles, which will enhance the colour, luminescent intensity and lifetime of such displays. His research led to the establishment of a strong group working on luminescent materials and to the establishment of several smaller groups all over South Africa. He has more than 830 publications in international peer reviewed journals, 120 peer reviewed conference proceedings and editor/author or co-editor/author of 80 book chapters and or books with more than 23200 cited author references, H-index of 67, i10 index of 563 on google scholar (51 and 434 since 2019) and more than 730 national and international conference contributions (authored and co-authored). He has an ISI H-and scopus index of 55 (rid = g–2696–2012) and 58, respectively. He is a reviewer for more than 100 international and national professional journals in his field (or in related fields), and a member of the editorial board of the high impact factor journal 'Critical Reviews in Solid State and Materials Sciences" (IF-10.367). He was awarded with the Institutional Research Development programme award for the Highest scoring RNA on Nano Solid State Lighting in 2007 (NRF). He has received the South African National Science and Technology Forum (NSTF) award in 2009 for research capacity development of students in the niche area of nanophysics. His commitment to the next generation of scientists is also reflected by the awards he received from the Faculty of Natural and Agricultural Sciences at the University of the Free State, South Africa for excellence (deans medal) (2012), research (2014), mentorship (2008), for academic entrepreneurship (2009), best researcher (2018). He received honorary membership of the Golden Key Association (2012). The Radio Rosestad, a local radio station, award for outstanding research and post graduate teaching in 2017. He received the Havenga Prize for original research from the South African Academy of Art and Science in 2022. He was chair of national and international conferences. He has supervised more than 110 PhD and MSc students successfully in the past with another 20 in progress and has established a National Nano Surface Characterization Facility (NNSCF) containing state of the art surface characterization equipment. A research chair in Solid State Luminescent and Advanced Materials was awarded to him from the South African Research Chairs Initiative (SARChI) at the end of 2012 which was renewed for another 5 years at the end of 2017 and again at the end of 2022. The main focus of his research group is the improvement of luminescent materials for applications in flat panel displays, solar cells, solid state lighting, dosimetry, and thermometry.

© 2024 The Authors. ChemElectroChem published by Wiley-VCH GmbH

density without sacrificing power density or even enhancing the electrochemical features and efficiency of SCs so the energy density reaches that of batteries with superior power and cyclic performance.[5] Developing new materials and understanding electrochemical interfaces at the nanoscale are crucial. The large electrochemically active surface of 2D materials, such as graphene, makes them attractive for SC electrodes.[13] The layered structure allows intercalation of foreign species, altering structural properties and causing volumetric expansion. 2D layers, being atomically thin with a large surface area, result in higher electrochemical activity.[14] While graphene dominates 2D material research, its practical applications are hindered by its carbon networking. Layered materials with more than one element offer diverse structural arrangements tailored for specific characteristics.[15–23] Nanostructures derived from 2D materials present several key advantages, with their highly exposed surface and edge active sites and their weak van der Waals (vdW) interaction providing efficient intercalation of guest species.[24] Natural and post–synthesized 2D materials like graphene, boron nitride, TMDCs, MAX phases, and 2D Metal–organic frameworks have been obtained using various techniques.[25–33] The combination of crystal structures and phases significantly impacts the electrochemical characteristics of 2D materials. Owing to the different phases and oxidation states of TMDCs, they exhibit high electrochemical characteristics and potential widening.[34] The MXenes have recently gained popularity as promising candidates for SCs electrodes since they have a high surface area, are intrinsically highly conductive, and are electrochemically active, which makes them ideal for intercalation pseudocapacitance.[35] Significant progress has been made in obtaining nanostructured, highly defective, and metastable materials, where pseudocapacitive behaviour is explained by structural features. Pseudocapacitive responses can be caused by features such as confined interlayer fluids in two–dimensional materials. An in–depth discussion of the history and mechanisms of pseudocapacitive 2D materials, focusing on their electrochemical characteristics through in situ or operando studies, provides a deeper comprehension of pseudocapacitance. Developments of 2D materials facilitates pseudocapacitance intercalation, promoting energy and power densities enhancement in SCs.[11–36]

2. Charge Storage Mechanisms in SCs

SCs are defined by their electrostatic or Faradaic processes, representing high–speed electrostatic or Faradaic redox mechanisms. The surface of electrodes plays a key role in controlling the number of charges accumulated at the interfaces, exploiting its high surface area. SCs consist of two electrodes comprising highly porous materials immersed in electrolyte, isolated by an ion–penetrable and nonconductive separator. The incorporation of SCs electrode materials with higher surface area, in contrast to conventional electrodes, along with nanoscale dielectric distances, significantly enhancing specific capacitance and energy densities, reaching values that are 1000 times higher than conventional capacitors.

Regular capacitors and supercapacitors employ the same charge storage mechanism, but the significantly higher surface area and porous nature of SCs′ electrode surfaces enable the storage of many charges. This characteristic enhances energy density, which is possible through the incorporation of highly nanoporous materials with high surface area in SC electrodes, facilitating pseudocapacitance/faradic redox reactions. This integration results in specific capacitance values ranging from 10^2–10^3 F/g.

Batteries and supercapacitors stand as prominent energy storage devices in practical applications, differing in their energy density and power density based on charge storage mechanisms. Due to their high–power density, SCs are highly preferred in high–power systems requiring rapid energy delivery within seconds to minutes. While SCs exhibit electrochemical behaviour akin to batteries, distinguishing features include high power density, extended cycle life, tolerance to high operating temperatures, and rapid charging–discharging.

In contrast to batteries, SCs display a linear potential increment during charging–discharging with a constant current, indicating charges accumulate on the electrodes. The rectangular shape of the cyclic voltammetry (CV) curve for SCs illustrates potential–independent capacitance, maintaining a constant current during redox reactions (Figure 1a). Batteries, conversely, show distinct spikes denoting Faradaic reactions (Figure 1b). Galvanostatic charge-discharge curves for SCs reveal steep slopes and a consistent incline on their curves (Figure 1c), while batteries typically exhibit a relatively flat charge/discharge profile under constant voltage (Figure 1d). An electrode's capacitance ultimately determines the amount of charge that can be stored at a given voltage.

$$C = \frac{\Delta Q}{\Delta V} \tag{1}$$

In Equation (1), the capacitance is C, ΔQ is the charge stored and ΔV is the applied potential. The capacitance value is determined by the unit of Farad (F).

The charge storage mechanisms in SCs can be divided into two categories: EDLCs and pseudocapacitors. Charges are stored in EDLCs by adsorbing ions onto their surfaces Figure 2a. The absence of redox reactions in EDLCs results in rapid potential perturbations, leading to high power densities. However, the EDLC mechanism solely involves surface charges, resulting in relatively low energy density values. The EDLCs based specific capacitance are driven by their electrodes surface area, porosity, and surface properties, particularly those featuring larger surface area and high conductivity.[38,39] The EDLC diagram illustrates the accumulation of charges at the electrode/electrolyte interface through electrostatic adsorption, typically within atomically thin layers in the range of 5–10 Å,[40] creating differentiation between opposite charges.[41]

In the EDLC, capacitance is calculated as follows,

$$C = \frac{\varepsilon_r \varepsilon_0}{d} A \tag{2}$$

© 2024 The Authors. ChemElectroChem published by Wiley-VCH GmbH

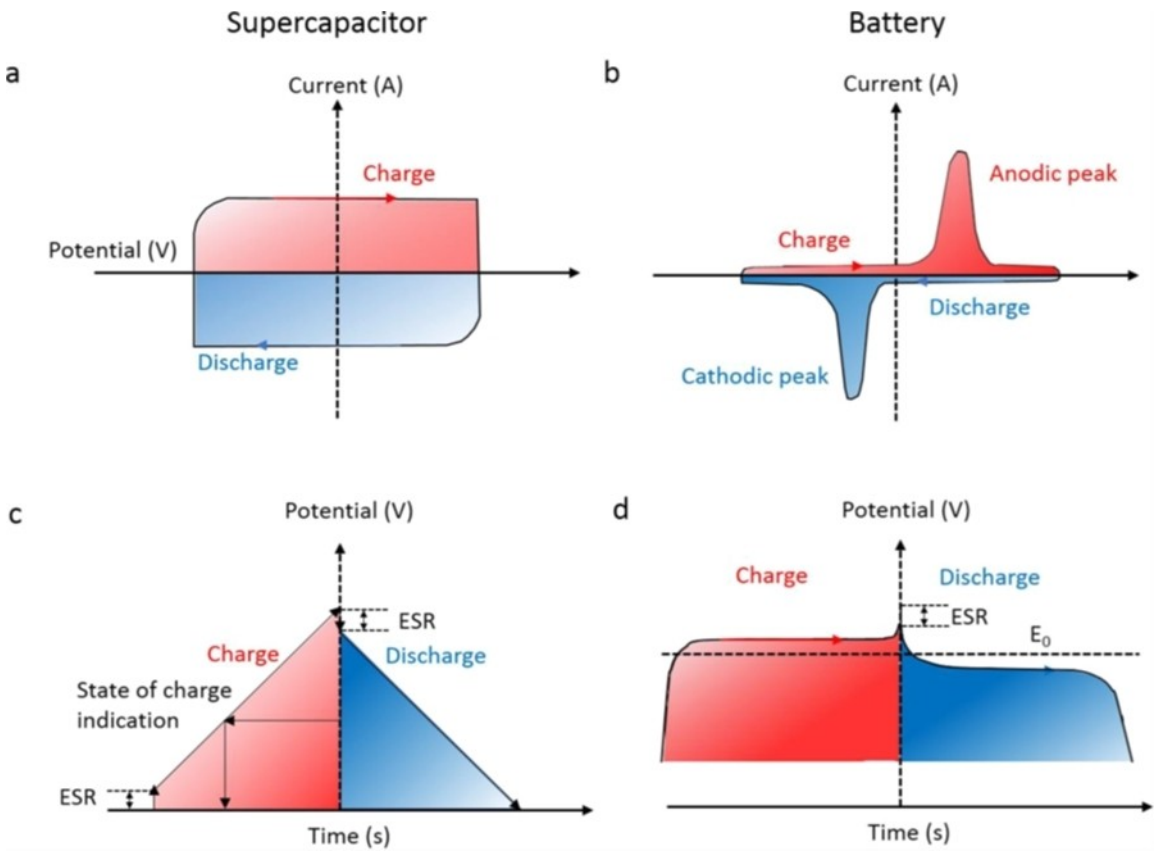

Figure 1. Evaluation of electrochemical characteristics of SCs and batteries: ((a) and (b)) CV and ((c) and (d)) GCD curves reprinted from ACS *Chem. Rev.* **2018**, *118(18)*, 9233–9280, Copyright © 2018, American Chemical Society.[37]

In Equation (2), ε_r is the relative permittivity associated with the electrolyte, and ε_0 (8.854×10^{-12} F/m) is the permittivity of vacuum and A is the electrode surface area, and d is the Debey length.

2.1. Pseudocapacitance Charge Storage Mechanisms

The term "pseudocapacitance," introduced by David C. Grahame in 1941,[42] was later adopted by Conway and Gileadi during 1960s proposed electrochemically reversible capacitance not associated with EDLCs.[43,44] Pseudocapacitance is determined by adsorbates on surfaces, resulting from distinct Faradaic redox reactions compared to EDLCs. Unlike EDLCs, pseudocapacitive electrodes depend on swift and reversible Faradaic redox reactions on the electrode surfaces, involving electron transfer events that modify the valence state of the electrode material.[9] In essence, pseudocapacitance denotes materials displaying capacitive electrochemical properties while storing charge through charge–transfer Faradaic reactions across their double layers.[45] In energy storage with pseudocapacitance, the electrochemical activity aligns with pure electrostatic EDLCs, and bulk battery–type diffusion controlled by Faradaic redox kinetics. Faradaic redox reactions are categorized based on capacitive mechanisms, including underpotential deposition, redox pseudocapacitance, and intercalation pseudocapacitance.

2.2. Underpotential Deposition Pseudocapacitance

The underpotential mechanism involves Faradaic adsorption/desorption on metals, originating from reversible surface chemisorption.[46] Metal ions predominantly form underpotential ions when they create monolayers on surfaces with higher redox potentials. The rapid electron kinetics in the electrochemical process, facilitated by the surface–adsorbed species, leads to underpotential deposition. This results in the electroplating of metals both on the materials and the underlying metal electrode, leading to partial electron transfer. For instance, the underpotential deposition pseudocapacitance is illustrated by the deposition of Pb^{2+} on the gold (Au) surface.[47] The underpotential mechanism of noble metals can be elucidated by the Equation (3) Figure 2b, as follows:

$$M + xC^{z+} + xze^{-} \leftrightarrow C.M \tag{3}$$

where *M* represents the metal atoms, *z* denotes the valency of adsorbents, x signifies the number of adsorbents, and C refers to the adsorbents. Therefore, xze^{-} is indicative of the number of electrons transferred. In pseudocapacitance, the significance of rapid and reversible redox reactions is paramount for achieving high power density. However, it's worth noting that underpotential deposition is associated with relatively low voltage values, typically around 0.6 V, leading to lower energy densities.

© 2024 The Authors. ChemElectroChem published by Wiley-VCH GmbH

2.3. Redox Pseudocapacitance

Another pseudocapacitance mechanism, known as redox pseudocapacitance, emerges from redox reactions involving Faradaic electron transfer kinetics at electrode–electrolyte interfaces. This pseudocapacitance has been observed in materials like ruthenium oxide, which encompasses +2, +3, and +4 oxidation states.[48] In the redox pseudocapacitance mechanisms, electron transfer occurs between oxidized (Ox) and reduced (Red) species. Cations are electrochemically adsorbed onto oxidized species during these rapid and reversible redox reactions, and this chemical process can be expressed through the following equation (4).

$$Ox + zC^{+} + ze^{-} \leftrightarrow RedC_{z} \quad (4)$$

Where C denotes alkali metal ions present on electrolytes, which undergo adsorption onto the surfaces, and ze^{-} denotes amount of electrons involved in redox reactions Figure 2c. Redox pseudocapacitance has been identified in materials such as RuO_2, where charge storage occurs due to protons in a Faradaic nature. This phenomenon is associated with the +4 oxidation state of ruthenium, featuring higher conductivity and shorter diffusion path lengths.[49]

Redox pseudocapacitance is an electrochemical reaction in which ions are absorbed onto materials with a Faradaic charge transfer, commonly observed in aqueous electrolytes, including widely used materials like MnO_2 and RuO_2.[48–51] In pseudocapacitive electrodes, the electrochemical characteristics are classified based on faradaic redox reactions, exhibiting rectangular CV shapes or wide peaks with small voltage differences and a sloped charge–discharge curves.

2.4. Intercalation Pseudocapacitance

The last pseudocapacitance mechanism is intercalation pseudocapacitance, which is caused by ions intercalating at the layers or tunnels of electrodes, leading to Faradaic charge transfer without crystallographic phase changes. Afterwards, the process is further elaborated in the subsequent section. Intercalation pseudocapacitance manifests in systems where ions are intercalated into redox-active materials without altering their crystallographic phase. In contrast to surface redox reactions, intercalation pseudocapacitance emerges more from thicker electrodes.

The intercalation pseudocapacitance mechanism is illustrated in Figure 2d, expressed as follows (refer to Equation (5)),

$$MA_{y} + xLi^{+} + xe^{-} \leftrightarrow LixMA_{y} \quad (5)$$

Where xe^{-} represents the quantity of charges transmitted and MA_y denotes the layer/lattice intercalation with electrode material. In addition, such crystalline lattices in electrode materials enable alkali metal ions to intercalate with the least energy constraint, leading to minimal modifications.

2.5. Importance of Intercalation Pseudocapacitance

Generally, pseudocapacitor materials exhibit high capacitance and rapid charge/discharge abilities, leading to considerable efforts in designing various materials for supercapacitors. According to this concept, pseudocapacitance emerges on the surfaces of materials where redox reactions are reversible, representing a faradaic nature distinct from EDLCs. The pseudocapacitive properties of electrode materials are rooted in the Faradaic process occurring at or near their surfaces, giving rise to the term "pseudocapacitive materials." Capacitance results from the unique interplay between charge acceptance

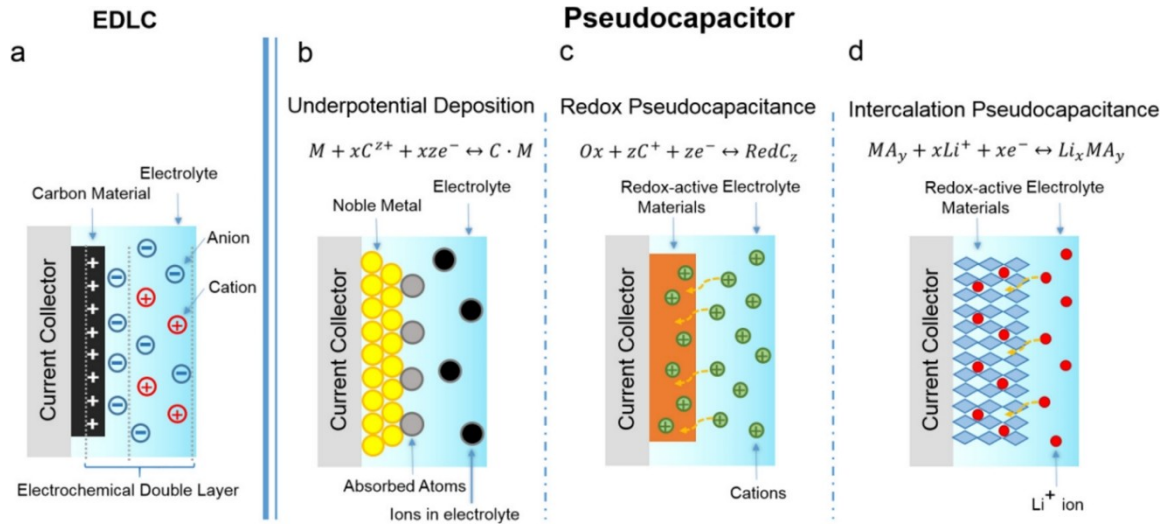

Figure 2. An illustration of the charge storage mechanisms (a) EDLCs and (b) Underpotential deposition, (c) Redox Pseudocapacitance, (d) intercalation pseudocapacitance reprinted from ACS *Chem. Rev.* **2018**, *118(18)*, 9233–9280, *Copyright © 2018, American Chemical Society*.[37]

© 2024 The Authors. ChemElectroChem published by Wiley-VCH GmbH

(Q) and potential change (V), where △Q/△V is equivalent to capacitance.[47,52]

While oxidation–reduction reactions form the basis of charge storage, electrode materials exhibit behavior similar to batteries. However, electrochemical signatures are characterized by (near-—) rectangular cyclic voltammograms (CVs) and near–linear galvanostatic charge–discharge (GCD) curves, indicating faradic reactions unaffected by diffusion in solid states. Despite charge storage occurring on the electrode surface, EDLC is not a Faraday process. The Faradaic reaction establishes a clear distinction between capacitance and pseudocapacitance, hence the term "pseudocapacitance" Pseudocapacitors encompass materials like transition metal oxides (MnO_2), ruthenium oxides (RuO_2), and iron oxides, particularly in aqueous solutions with a large potential window. The reaction kinetics in pseudocapacitive materials generally outperform those in batteries. Extensive research on electrodes made from nanomaterials over the past decades has revealed that their specific surface area far exceeds that of bulk battery materials. Consequently, the diffusion time of ions has been significantly reduced, transforming the "bulk redox reaction" into a "surface redox reaction," as elucidated by Dunn and Simon et al through a novel mechanism.

Intercalation pseudocapacitance, a phenomenon commonly observed in non-aqueous electrolytes, involves ions intercalating into electrode layers of redox active electrode materials.[9] Unlike surface reactions, intercalation pseudocapacitance ensures the stability of redox reactions, allowing alkali metal ions present in the electrolytes to penetrate through supercapacitor electrodes. Nevertheless, electrode materials exhibiting intercalation pseudocapacitance still exhibit distinct CV peaks. Studies suggest that the intercalation process in batteries is fundamentally restricted as ions diffuse into their bulk phases. In all these situations, there exists a correlation between the degree of charge storage (X) and the potential (E).

$$E \approx \frac{RT}{nF} \ln\left(\frac{X}{1-X}\right) \tag{6}$$

In Equation (6), R denotes the ideal gas constant ($J\,mol^{-1}\,K^{-1}$), T is the temperature (K), F is Faraday's constant ($96{,}485\ As\,mol^{-1}$) and n is the number of electrons involved in the reaction. In all of these cases, a constant–current experiment yields a potential E that changes with the extent of charge Q according to:[53]

$$Q = C\Delta E \tag{7}$$

In Equation (7), Q denotes charge transferred (Coulombs), E denotes potential difference (V) and C denotes pseudocapacitance (F). It is characteristics of capacitive charge/discharge, resulting in the concept of pseudocapacitance. The pseudocapacitance generated from, underpotential deposition and surface redox reaction pseudocapacitance are characterized by electrochemical processes controlled by the surface.

$$i = Cv \tag{8}$$

In Equation (8) I is the current (A) and v is the sweep rate ($mV\,s^{-1}$) of a CV measurement.

Quantification plays a pivotal role in comprehending pseudocapacitance phenomena. Additionally, many electrochemical redox reactions are assessed CVs, GCD, and electrochemical impedance spectroscopy (EIS), which rely on ion diffusion mechanisms. In a redox reaction regulated by ion diffusion, the current will fluctuate depending on the sweep rate. Various methods have been suggested to differentiate between diffusion–controlled and non–diffusion limitation mechanisms for supercapacitor electrode surfaces (refer to Equation (9)).

$$i(V) = k_1 v + k_2 v^{1/2} \tag{9}$$

V represents potential, v refers to the sweep rate (mV/s), k_1 and k_2 are determined by the diffusion and capacitive currents. A simplified version of this formula is as follows:

$$i(V) = av^b \tag{10}$$

A quantitative analysis of diffusion–controlled and capacitive contributions was proposed by calculating b (Equation (10)). If the b value is 0.5 describes that the materials are pseudocapacitive (a diffusion–controlled faradaic mechanism) (e.g., TiO_2, MoO_3, Nb_2O_5 and various MXenes) and for the b value is 1 indicates that the kinetics are controlled by surface. This mechanism has been extensively employed for studying the kinetics of various nanomaterials surface for the SCs electrodes.

To accurately distinguish pseudocapacitance from battery behavior, we propose an approach that considers both electrochemical characteristics, such as CVs and GCD, along with quantitative kinetic analysis (calculation of b from Equation (10)), as illustrated in Figure 3. The curve for the EDLC mechanism is included for comparison. EDLCs material demonstrates a rectangular type CV and GCD with a linear potential concerning time, where b equals 1 refer to Figure 3a.

Pseudocapacitive materials are expected to display approximately rectangular CVs, potentially showing inflections, but not flat curves, with b approximately equal to 1 refer to Figure 3b. Conversely, in batteries, CV generally reveals redox peaks, and GCD demonstrates plateaus (b = 0.5) refer to Figure 3c. To exhibit a distinct electrochemical signature, pseudocapacitive materials should showcase multiple scan rate and current density values, regardless of material size or thickness. Through quantitative analysis, it has been recognized that high–rate CVs may not be suitable due to the significant ohmic drop, especially when the b value is 1. The value of b is 1 not only signifies capacitive processes like EDLC or pseudocapacitive but also indicates a process independent of ion diffusion based on the specific material structure.

Based on the preceding discussion, two common SCs, namely asymmetric SCs and hybrid SCs are described. As depicted in Figure 4a, four potential configurations are considered for asymmetric supercapacitors, involving combinations of EDLC and pseudocapacitance electrodes with opposite polar-

© 2024 The Authors. ChemElectroChem published by Wiley-VCH GmbH

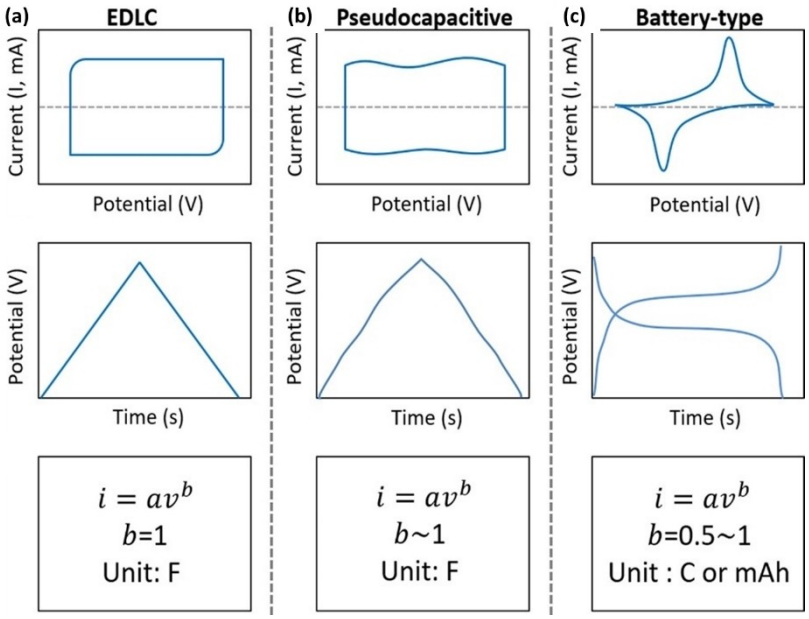

Figure 3. A standard electrochemical behavior that classifies the EDLC, pseudocapacitance as well as batteries reproduced with permission copyright 2019 John Wiley and Sons.[52]

ities (e.g., EDLC + ve and pseudocapacitance −Ve electrode, EDLC −ve and pseudocapacitance + ve). Here, EDLC + ve (A) and EDLC −ve (B) electrodes are defined as A not equal to B, and the same principle applies to pseudocapacitive + ve and −ve electrodes. For hybrid supercapacitors, various assemblies include EDLC (+ ve) and battery–type (−ve) electrode, battery–type (+ ve) and EDLC (−ve) electrode, battery–type (+ ve) and pseudocapacitive (−ve) electrode, and pseudocapacitive (+ ve) and battery–type (−ve) electrode, incorporating aqueous and non-aqueous electrolytes, as well as gel electrolytes. These devices, aiming for charge balance and optimal use of positive and negative materials, exhibit minimal redox peaks. The charge storage mechanism, based on ion intercalation techniques, encompasses Faradaic effects arising from solid-state diffusion, rapid Faradaic charge transport mechanisms at the electrode surface, and EDLC charge transfer due to electron electrostatic ion adsorption/desorption.[54] Thus, to determine the number of charges stored, it is imperative to distinguish between capacitor contributions and Lithium–ion intercalation processes.

The charge–storage system demonstrates enhanced capacitance when the active surface area is exposed, and the ion

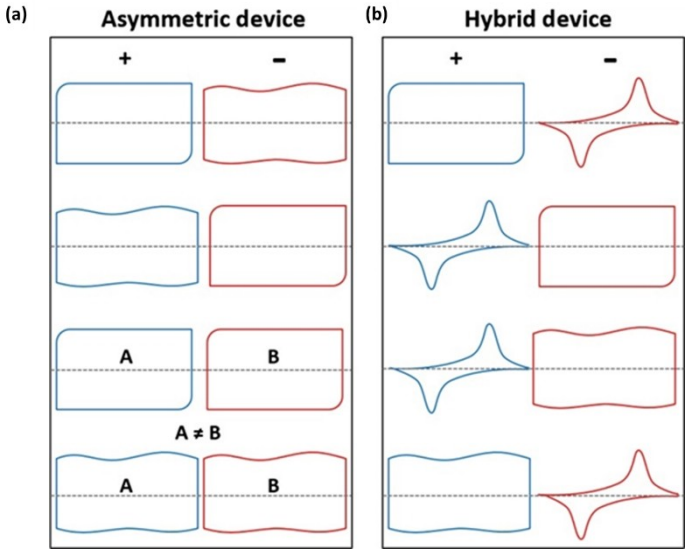

Figure 4. Asymmetric and hybrid supercapacitors with different CV characteristics (A and B are two types of materials reproduced with permission copyright 2019 John Wiley and Sons.[52]

© 2024 The Authors. ChemElectroChem published by Wiley-VCH GmbH

diffusion distance is minimized. Pseudocapacitance, occurring at electrode surfaces 10 to 100 times larger than EDLCs, is particularly prominent in asymmetric supercapacitors based on redox pseudocapacitance or intercalation pseudocapacitance. Emphasizing these considerations, it is crucial to apply discussions of pseudocapacitive behavior to individual electrodes. Combining capacitive electrodes with Faradaic electrodes makes it challenging to determine whether they are associated with pseudocapacitors or batteries. CV curves may still resemble rectangular shapes even when combining a battery–type electrode and a capacitive electrode.The significance of intercalation pseudocapacitance surpasses that of underpotential and redox pseudocapacitance. Its capacitor–like electrochemical characteristics, such as rapid charge transport, fast charging duration within seconds, higher charging/discharging rates, enhanced stability, and high–power density, differentiate it from typical battery materials. However, supercapacitors are constrained by their lower energy density compared to batteries. The introduction of the intercalation pseudocapacitance mechanism in supercapacitor electrodes can overcome this limitation, and its occurrence is influenced by the grain size and morphology of electrode materials. In bulk electrode materials, it is termed intrinsic intercalation pseudocapacitance, while nanostructured electrode materials contribute to extrinsic pseudocapacitance processes.

The primary feature of intercalation pseudocapacitance lies in its potential that connecting lithium–ion batteries and supercapacitors, offers both high power and energy density.[55,56] Combining EDLCs with redox reactions in pseudocapacitance increases the amount of charge that can be stored. A diverse range of pseudocapacitance materials has been developed, including metal oxides, sulphides, nitrides, and carbides. Each material exhibits a distinct pseudocapacitance mechanism, providing the possibility of delivering a combination of battery–like higher energy density and EDLC–like higher power densities, along with higher cycle stability. The term "pseudocapacitors" is employed for supercapacitors to avoid confusion with EDLCs, encompassing charge storage process and the materials involved. Designing appropriate electrode materials for intercalation pseudocapacitance to deliver high power and energy density with higher stability suggests a promising future for supercapacitors.

3. Advanced Materials for Supercapacitor Electrodes

Supercapacitors are continually advancing in terms of functionality, employing diverse materials as their fundamental components, and adopting various synthesis methods. Oxide materials show significant potential in intercalation pseudocapacitance. For instance, mesoporous $RuO_2 \cdot xH_2O$-based pseudocapacitance electrodes demonstrate an impressive capacitance of 1000 F/g, attributed to the hydrophilic surface facilitating efficient H^+ ion diffusion and effective charge storage.[57] Similarly, mesoporous Nb_2O_5, with short diffusion paths and exposed edges due to interlayer distance, exhibits efficient Li^+ ion intercalation, resulting in rapid redox intercalation pseudocapacitance.[58] Kim et al. observed capacitance value is 400 F/g within a short duration for Nb_2O_5,[59] and MoO_3[60] also exhibit promising properties. However, these oxide materials face limitations such as poor charge/discharge rates and small potential ranges, leading to suboptimal energy density values. The inadequate conductivity of oxide materials hampers their electrochemical performance, preventing access to deeper regions of the electrode materials during rapid kinetics.[61]

Layered materials with pseudocapacitive features can be achieved through nanoengineering electrode materials that combine diffusive and surface–dominated characteristics resembling both battery and capacitor behavior. While numerous materials are being investigated for supercapacitor electrodes, 2D materials has gained significant popularity in SCs. This is attributed to their remarkable electrochemical properties arising from high surface area with atomically thin layers and versatile morphologies with tunable electrochemical features. Through rational control of their surface chemical properties, 2D materials can enhance site–level storage capacity for electrons and ions, contributing to their superior electrochemical performance.[62]

4. Electrochemical Properties of Layered 2D Materials

When the structural properties of a material change, it can acquire novel and exciting characteristics, leading to unique physicochemical properties in atomically thin 2D materials compared to their counterparts. In monolayer 2D materials, the confinement of electrons within their 2D space enables intriguing optoelectronic properties, making them ideal for applications in optoelectronics.[63] The strong covalent bonds along the plane between atoms in a monolayer provide both high mechanical strength and flexibility, along with transparency with enormous surface area arehighly favourable which are intended for numerous optoelectronic devices.[64]

Utilizing 2D layered nanomaterials, supercapacitors can achieve intercalation pseudocapacitance that offer substantial charge storage capacities without the limitations imposed by solid–state diffusion. The transport kinetics of ions in supercapacitors are closely linked to the choice of electrode materials. Pseudocapacitors show great promise in merging the void among batteries and SCs. 2D structures have significant scientific and technological implications, particularly in SCs, where they can exhibit intercalation pseudocapacitance with exceptionally high charge storage capacities in a short duration, despite limitations posed by solid–state diffusion.[50]

Novel 2D materials are being explored in light of graphene discovery with extraordinary physicochemical properties has led to the identification of materials like TMDCs, TMOs, MXenes and 2D MOFs. These materials find widespread applications in electrochemical devices, owing to their unique electrochemical properties. The figure below illustrates the charge storage

© 2024 The Authors. ChemElectroChem published by Wiley-VCH GmbH

mechanisms among pseudocapacitance, rechargeable batteries, and capacitors.[65] Our focus will be on exploring the electrochemical features of 2D materials, their advancements, and the challenges associated with redox reactions in pseudocapacitance intercalation for supercapacitors.

4.1. Graphene in SCs

Although graphene's properties are closely related to how it is prepared. The monolayer graphene sheet is typically made of carbon atoms in a hexagonal lattice structure holds a high surface area ~2630 m^2/g and a high mechanical strength of up to 1 TPa exhibited high electrical conductivity and better electrochemical properties demonstrates SCs with a fast rate of redox reactions and excellent cycle stability. The monolayer graphene exhibits with intrinsic capacitance of ~21 $\mu F/cm^2$ and achieved the gravimetric capacitance of ~550 F/g. Graphene opens up new possibilities in electrochemistry and electrochemical devices with potential benefits. The active sites sp^2 and several defects present in graphene is directly impact on the energy and power density of the SCs.[66] Upon measuring the capacitance of monolayer graphene, the charges accumulated simultaneously on both sides of the graphene sheets were significantly lower than on the single side. A possible explanation for such an observation was that the capacitance of single–layer graphene displayed quantum effects[67] so the general synthetic route of graphene, contributing significant impact on overall capacitance of the SCs.[68–70] The amount of wrinkled nature, pores and a number of layers in graphene also determines the specific capacitance value of SCs. For instance, Lena et al. demonstrated that wrinkled graphene oxide demonstrates higher capacitance of 211 F/g,[71] whereas Meryl et al. demonstrated the defective graphene shows 100 F/g.[72]

The available surface area and ion diffusion rate of 2D graphene are reduced greatly by its ability to restack during its processing process. This reduces its specific capacitance and rate performance.Due to weak vdW interactions, stacked structures forming by the stacking layers together greatly influences charge transfer behaviours. With numerous efforts, layer stacking can be stabilized with the help of surfactants for stable dispersibility,[73] and by introducing heteroatom dopants.[74,75] Kai et al. utilized TBOAH as a stabilizer on graphene, obtained a specific capacitance of 195 F/g with the highest stability.[76] Mao et al. demonstrated the combination PANI with graphene high specific capacitance of 526 F/g achieved at 0.2 A/g over wide range of cycles.[77] It is possible to alter graphene's electronic structure by doping it with heteroatoms and other internal properties, where the boron (B) dopants[78] make the graphene n/p type, and nitrogen (N) dopants[79–81] create an electron donor and polarization in the sp^2 carbon network and sulphur (S) dopants[82,83] improves the electrocatalytic activity of graphene.

The pseudocapacitance behaviour can be achieved in graphene-based SCs by either combining them with TMOs or conducting polymers. Graphene composites with varying materials can store an enormous amount of electrical charge and exhibit pseudocapacitance through a fast–faradaic redox reaction, the pseudocapacitance of supercapacitors increases due to charge transfers atelectrolyte–electrode.[84] The most common pseudocapacitive features arises based on TMOs. Xiang et al. achieved TiO_2 with reduced graphene oxide (rGO) with a specific capacitance value of 225 F/g.[85] A hybrid SCs with high energy density values has been achieved by Kim et al. with anatase TiO_2 with rGO and exhibited the specific capacitance value of 53 F/g.[86] Xiang et al. achieved specific capacitance value of 472 F/g by using a nanocomposite of rGO with cobalt oxide (Co_3O_4).[87] Yue et al. synthesized rGO/Co_3O_4 composite by hydrothermal route that demonstrated specific capacitance of 1152 F/g.[88] Soam et al. developed paper like flexible Graphene/bismuth Ferrite composite for flexible SCs and demonstrated specific capacitance value of ~18 mF/cm.[2,89] Qu et al. used Fe_3O_4@RGO nanocomposites for SCs electrode that exhibited higher capacitance (326 F/g).[90] Sun et al. prepared electrode material by atomic layer deposition method and exhibited specific capacitance of 84 F/g.[91] Likewise, conducting polymer nanocomposites with graphene shows pseudocapacitance behaviour.[92,93] It has been demonstrated that graphene and its derived materials, such as rGO and graphene with dopant, features a rich electrochemical property.

4.2. 2D Transition Metal Oxides

The 2D transition metal oxides (TMOs)) are the widely used active SCs electrode materials with high availability, demonstrating theoretically high capacitance as well as high energy density values. As an ultrathin nature of TMOs are possess high electronic conductivity which is highly beneficial for decreasing the ionic resistance in the diffusion process.[94] A number of approaches are being studied in TMOs to develop highly efficient electrode materials for SCs, including anion intercalation. 2D nanostructures are highly preferable in terms of their sheet-like structure as electrodes that do not require substrates. Lubimtsev et al. utilized *ab initio calculation* to understand the pseudocapacitance intercalation in the layered niobium pentoxide (Nb_2O_5) particularly in orthorhombic and monoclinic phases. Upon intercalating with Li+ atoms in 2D Nb_2O_5, donating the electrons to the local nearby atom to reduce Nb (Equation (11)).[95]

$$Nb_2O_5 + xLi^+ + xe^- \leftrightarrow Li_xNb_2O_5 \tag{11}$$

Liu et al. synthesized flower like V_2O_3 by using solvothermal technique, which demonstrated the specific capacitance value of 218 F/g.[96] the Li^+ ion insertion/extraction can be described as follows (Equation (12)),

$$V_2O_3 + xLi^+ + xe^- \leftrightarrow V_2O_{3-x}(OLi)_x \tag{12}$$

The molybdenum trioxide is another SC material, that demonstrates the pseudocapacitance intercalation owing to its layered structure. The MoO_3 exist in two polymorphs such as thermodynamically highly stable orthorhombic α-MoO_3 and

© 2024 The Authors. ChemElectroChem published by Wiley-VCH GmbH

monoclinic β-MoO_3. Among them, the α-phase is a 2D layered structure with weak vdW interactions among layers which are highly beneficial for accommodating the ions for intercalation/deintercalation in SCs. Brezesinski et al. synthesized α-MoO_3 by arc evaporation techniques and used it for the Li^+ intercalation in SCs. The layered nature provides the accessibility of the intercalated molecules resulting in intercalation pseudocapacitance behaviour.[97] Lu et al. used seedlike mesoporous MoO_{3-x} nanosheets, the specific capacitance value of 1480 F/g with intercalation pseudocapacitance of H^+ ions.[98] The most efficient TMOs are nickle oxides and their derivatives for the SCs in intercalation pseudocapacitance with theoretically obtained specific capacitance value of 2584 F/g which is environment–friendly, low cost highly stable electrod e material.[99]

4.3. Transition Metal Dichalcogenides

Transition metal atoms are introduced amongst two chalcogen atoms to create the monolayer structure of TMDCs. Weak vdW forces bind adjacent layers together in bulk TMDCs. The sheet–like 2D structure of TMDCs presents two distinct electrochemical properties based on the surface–active sites, namely inert and highly active edge sites.[100] Consequently, the electrochemical properties of TMDCs differ based on the active sites of their basal and edge planes. Since the conductivity along monolayers is several thousand times higher than the bulk and the vdW force between layers allows heterogeneous electrons move more quickly along the edges than in the basal planes. In addition to the layers, TMDCs are characterized by their electrical conductivity through the arrangement of atoms in various polymorphs. TMDCs exhibit three different polymorphs, denoted as 1 T, 2 H, and 3 R, where the numbers indicate the layer count in a unit cell, and the letters refer to symmetry (T = tetragonal, H = hexagonal, and R = rhombohedral). Although devices based on TMDCs are rapidly advancing, our understanding of their intrinsic properties has not kept pace. Therefore, studying this aspect is crucial, as changes in TMDC materials can impact their effectiveness during operation. Numerous studies have demonstrated that various TMDCs with diverse phases exhibit unique capacitive features, such as H-MoS_2 monolayers for EDLCs and 2H/1T MoS_2 in pseudocapacitors with aqueous electrolytes.

A critical aspect of supercapacitors lies in the electron kinetics during redox reactions. A comprehensive understanding of how electrons are transferred between an electrode surfaces and electrolytes, as well as the electronic state of the solid material (electrode), aids in deciphering the intricacies of SC operation. Figure 5 illustrates the charge and discharge behaviour of MoS_2 pseudocapacitance. During discharge, vacancies in Mo atoms are filled by free electrons, subsequent to reduction in the valence of Mo atoms. Simultaneously, electrolyte–ions are surface–bound through Coulomb attraction. The charge status is reversed during charging.[101] While most research on pseudocapacitors concentrates on TMOs, metal sulphides also serve serve the purpose of pseudocapacitors. Metal sulfides, such as TiS_2 nanoplatelets, exhibit significant charge storage due to weakened interactions between guest ions (e.g., Li^+) and the sulphide lattices compared to oxides. This reduced affinity enables faster ion migration through the lattice.[102,103] To enhance SCs, efforts focus on increasing energy density, and stability, and simplifying their structure, despite their already substantial power density. 2D nanomaterials, serving as electrodes or modified electrodes through 2D intercalation, offer advantages such as 2D transport channels within the crystal network, causing minimal structural modifications upon intercalation. This approach enhances the

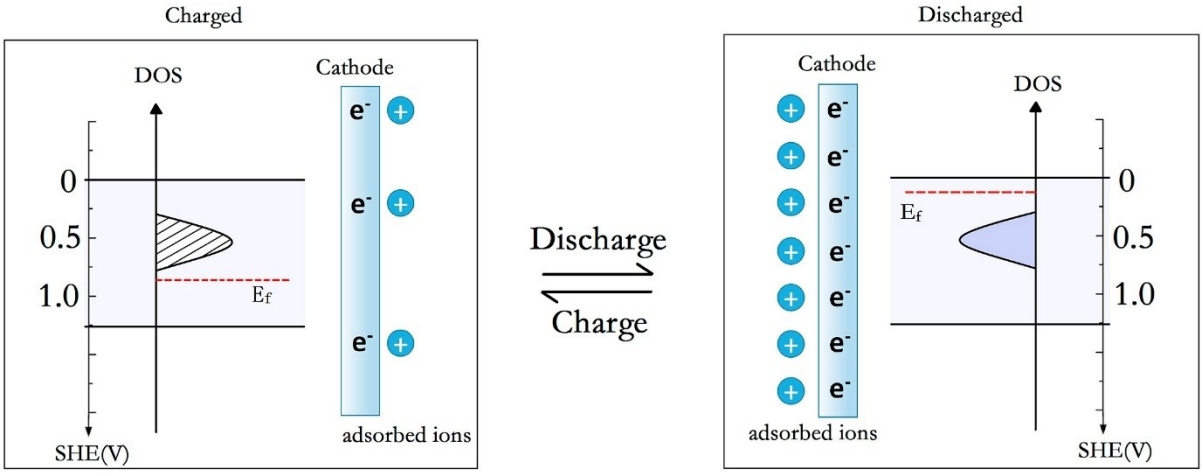

$$MoS_2 + A^+ + e^- \Leftrightarrow MoS\text{–}SA\ (A\ refers\ to\ H\ Li\ Na\ K\ etc.)$$

Figure 5. An illustration showing MoS_2's charge/discharge pseudocapacitance mechanism: electrons accepting and donating, and ions sorption and desorption. Fermi-level positions are indicated by red dashed lines. The pale blue area shows the potential window examined reproduced with permission[101] copyright 2016 Elsevier.

© 2024 The Authors. ChemElectroChem published by Wiley-VCH GmbH

durability of layered materials, contributing to the superior performance of high–performance supercapacitors.

4.3.1. Intercalation Pseudocapacitance in MoS_2

Multimorphic MoS_2, with its 1 T, 2 H, and 3 R phases, emerges as an appealing material for supercapacitor electrodes. However, optimizing its phase and stability is crucial to achieving maximum efficiency in capacitance performance. Exploring various ion-containing electrolytes such as Li_2SO4, Na_2SO_4, and K_2SO_4 has been instrumental in understanding the capacitance effects based on Li^+, Na^+, and K^+ ion intercalation in MoS_2–based electrodes. By intercalating these ions, MoS_2 experiences a significant expansion of the interlayer distance in MoS_2, a key factor influencing its energy storage efficiency.

In 2007, a chemical vapour deposition (CVD)-grown MoS_2 nano walls Figure 6a for SCs was introduced, exhibiting a specific capacitance of 100 F/g. This performance is resembles to the capacitance observed with carbon nanotube electrodes. However, this value decreases to 20 F/g at a scan rate of 50 mV/s. Faradaic reactions, including intercalated H^+ and Na^+ at the MoS_2 interfaces, are typically detected at slow scan rates due to the gradual nature of this process. At higher sweep rates, non–Faradaic mechanisms come into play Figure 6b–d.[104]

Being a 2D material, MoS_2 harnesses the vdW force to facilitate rapid intercalation of sodium ions (Na^+), thanks to its substantial interlayer distance ranging from 0.62 nm to an expandable 0.69 nm. The Na^+ intercalation pseudocapacitance presents a promising avenue for swift and cost–effective energy storage compared to lithium–ion systems. The layered vdW gaps, which attract Na^+, contribute to high ionic mobility and conductivity, particularly in the 1 T phase. An electrode, 30 microns thick and composed of 10–40 nm MoS_2 nanoparticles, showcases over 90 % capacitance retention.

In a series of kinetic analyses, the energy storage technique is elucidated, and its validity is corroborated by evidence from synchrotron based X-ray diffraction (XRD), indicates the material

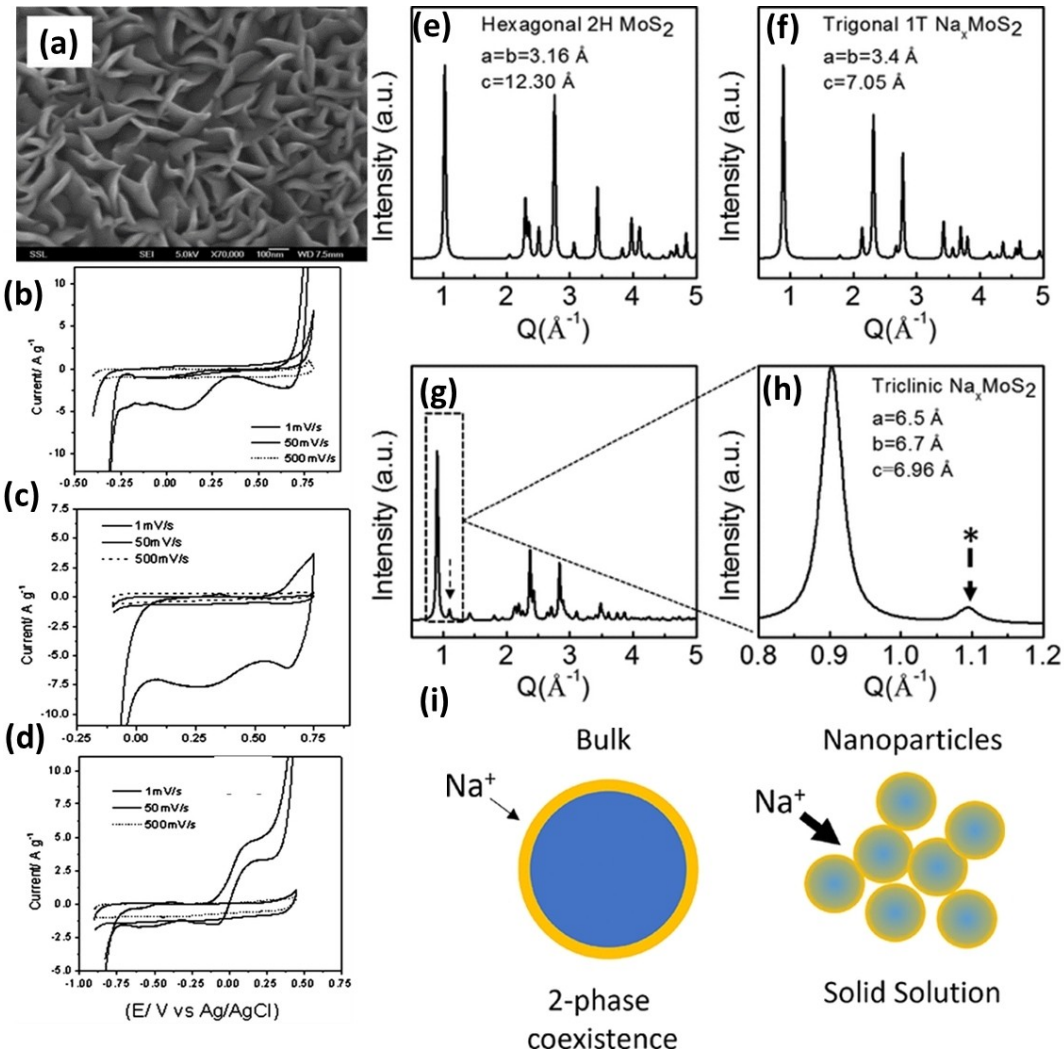

Figure 6. (a) SEM images of edge–oriented NWs and their CV at various sweep rates were collected in 0.5 M (b) H_2SO_4 (c) NaOH and (d) NaF concerning Ag/AgCl reproduced with permission[104] copyright 2007 IOP Science. Simulated PXRD of (e) $2HMoS_2$, (f) $1TMoS_2$, (g) Na_xMoS_2, (h) a dashed line separates (c)'s inset. *Triclinic peak at Q = 1.1 Å indicates (001) phase and (i) intercalation of Na^+ in bulk and nanoparticles of MoS_2 reprinted from *ACS Appl. Energy Mater.* **2023**, *6(1)*, 99–108[105] Copyright © 2023, American Chemical Society.

© 2024 The Authors. ChemElectroChem published by Wiley-VCH GmbH

undergoes nanostructuring, resulting in the suppression of a first-order phase transition. Notably, a phase transition occurs in MoS_2 from 2 H to 1 T as sodium ions undergo intercalation, and the galvanostatic traces of sodium ions inserted into 1 T–MoS_2 slowly replace them. Structural confirmation of this phase transition can be observed through XRD Figure 6e–h. The charge storage mechanism in MoS_2 with Na^+ intercalation Figure 6, i) is expressed by Equation (13), and this process is not confined to diffusion in solids.[104]

$$MoS_2 + xNa^+ + xe^- \leftrightarrow Na_xMoS_2 \quad (13)$$

Cook et al. successfully synthesized MoS_2 nanoparticles (NPs) with an expansion of atomically layered sheets, a crucial factor for the Faradaic redox mechanism, resulting in enhanced capacitance of 90 mAh/g within 20 seconds over 3000 cycles.[105] Generally, much of the research in supercapacitors based on MoS_2 has focused on augmenting the capacitance reaction, addressing its inherent poor reversibility. MoS_2–based electrode materials offer pseudocapacitive intercalation–based charging with rapid and highly reversible redox reactions, a phenomenon contingent on the thickness of the electrodes. Another notable advantage of MoS_2 is its ability to convert the 2H-phase into the 1 T conducting phase through the intercalation of Li^+ ions.[106–109] The conducting nature of the 1 T–Phase facilitates fast Faradaic redox reactions, albeit being thermodynamically unstable.[110] Thus, MoS_2 serves as an interaction host, offering a promising avenue for developing rapid charge storage devices with extended cycles. The intercalation/deintercalation of Li^+ ions with MoS_2 is described as follows (Equation 14).

$$MoS_2 + xLi^+ + xe^- \leftrightarrow Li_xMoS_2 \quad (14)$$

The intercalated lithium ions are situated at the octahedral sites of MoS_2.[111,112] Figure 6 b, d presents conclusive evidence demonstrating the transition from the 2 H to the 1 T phase resulting from the amalgamation of multiple nanoparticles (NPs). Wang et al. conducted a comprehensive investigation transformation of 2 H into 1 T phase in MoS_2, employing an atomic–level structural approach with Na^+ ions and high–definition scanning transmission electron microscopy (HD–STEM) images.[113] The structural characteristics of MoS_2 were affected by the quantity of Na^+ intercalated ions. In contrast to the conventional method of ascertaining the stoichiometry of intercalated ions through chemical means, STEM image analysis allows for an intricate exploration of MoS_2 structural progression with Na^+ ions on an atomic scale. The substantial insertion and extraction of Na, coupled with partial staging intercalation, uncover additional phase transition attributes of MoS_2.

Due to its layered structure, investigations have predominantly focused on the *c*-axis over *a* and *b* axes. The 2H-phase exhibits a hexagonal structure (S–Mo–S) with an ABA stacked arrangement, in contrast with its 1T-phase displays an ABC arrangementwith a (S–Mo–S_0) structure. These phases readily convert into each other through gliding between atomic planes within each layer, facilitated by the weak interaction involving the transversal displacement of one of the sulfur planes Figure 7a and b.

Wang et al.[114] introduced MoS_2–Carbon to establish an interfacial interaction with 2D layers, offering a potential solution to the significant challenge of fabricating high–performance energy storage devices by increasing active sites, enhancing electronic conductivity, and improving structural stability. Sodium (Na) contains three orders of magnitude more abundant than lithium (Li), providing effectively unlimited resources. Despite the larger size of Na^+ ions (>1.02 Å), the availability of anode materials for Na^+ storage is limited, posing challenges for sodium–ion capacitors that could be addressed through atomic interface modifications. Consequently, MoS_2–C achieved a high-energy density of 111.4 Wh kg^{-1} and maintained 77.3 % capacitance over 10,000 cycles with highly reversible characteristics, primarily due to the high volumetric capacitance of 1 T–MoS_2. Chen et al. explored the potential and frequency–dependent capacitance, achieving a capacitance of 94 F/g, which is 10 times higher than the 2 H-phase.[116]

Khawula et al.[115] utilized hydrothermally synthesized MoS_2–modified carbon nanospheres (MoS_2/CNS) as electrode materials for symmetric pseudocapacitors. When combined with CNS, MoS_2 becomes more conductive, demonstrating higher capacitance (231 F/g) and high energy density (26 Wh/kg) with a synergistic electrochemical capacitive behavior Figure 7, g–j, contributing to reversible redox reactions. The intercalation of sodium ions causes the exfoliation of MoS_2, resulting in a higher surface area capable of accommodating more ions, leading to increased capacitance and energy density. The intercalation of sodium ions is described by the following definition (Equation (15)).

$$MoS_2 + Na^+ + e^- \leftrightarrow MoS - SNa \quad (15)$$

Park et al. demonstrated the diffusion-controlled intercalation mechanism in MoS_2 within its heterostructure with RGO. The pseudocapacitive behaviour in an electrode is determined by the material's structure and physicochemical properties. Incorporating MoS_2 with RGO enhances its pseudocapacitive behaviour even further due to the rapid Faradaic charge transfer rate. The coupling of MoS_2 and RGO results in the creation of a 1 T phase at their interface, depicted in Figure 8a, providing an understanding of 2D hetero–nanosheet surfaces on electrochemical characteristics.[117] However, further clarification is needed regarding the surface redox reaction–based charge storage mechanisms in MoS_2 materials.[118–120]

When protons are introduced into the redox-active areas of MoS_2, reduction peaks in the electrons can be observed on CV curves Figure 8b as part of the Faradaic process. MoS_2/RGO achieved a capacitance value of 235 F g^{-1}, which is 1.7 times higher than 2 H–MoS_2 in the presence of H_2SO_4 electrolyte. Charge storage in 1 T MoS_2 is possible by inserting or removing H^+ from the interlayers and redox depositing it at the intralayer surfaces of the sheets, as explained in the equations (16) and (17).

© 2024 The Authors. ChemElectroChem published by Wiley-VCH GmbH

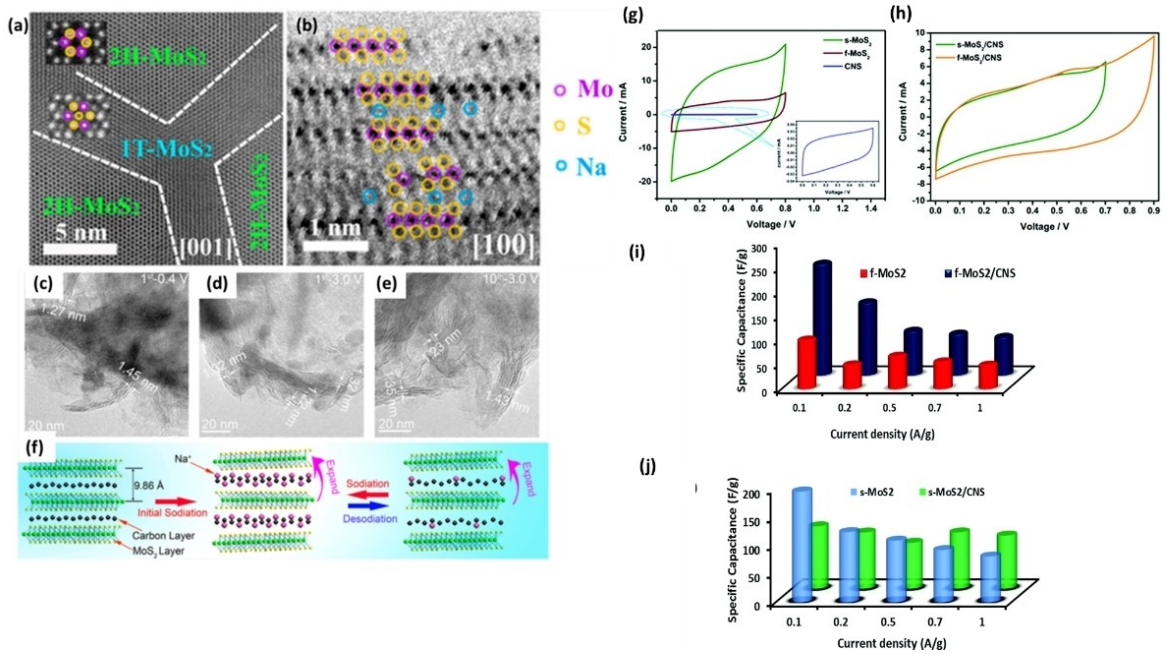

Figure 7. (a) STEM images of Na^+ intercalated MoS_2, the SAED reflecting crystallographic patterns of MoS_2 atoms arrangements. 1T phase formation by Na^+ intercalation along with (b) lattice distortion purple colour indicates the Mo atoms, yellow colour indicates the S atoms and blue colour represents the intercalated Na^+ ions adapted with permission *ACS Nano* **2014**, *8(11)*, 11394–11400[113] *Copyright © 2014, American Chemical Society.* The HR–TEM images show the MoS_2–carbon composite morphology of (c) initial sodiation (0.4 V) (d) during desodiation (3.0 V), following 10 cycles of desodiation (3.0 V) as shown. (g) and their corresponding schematic representation adapted with permission *ACS Appl. Mater. Interfaces* **2017**, *9(38)*.[114] *Copyright © 2017, American Chemical Society.* CV evaluation of (g) s–MoS_2, f–MoS_2 and CNS; (h) s–MoS_2/CNS and f–MoS_2/CNS and (i and j) their specific capacitance with various current densities[115] Reproduced from Ref.[115] with permission from the Royal Society of Chemistry.

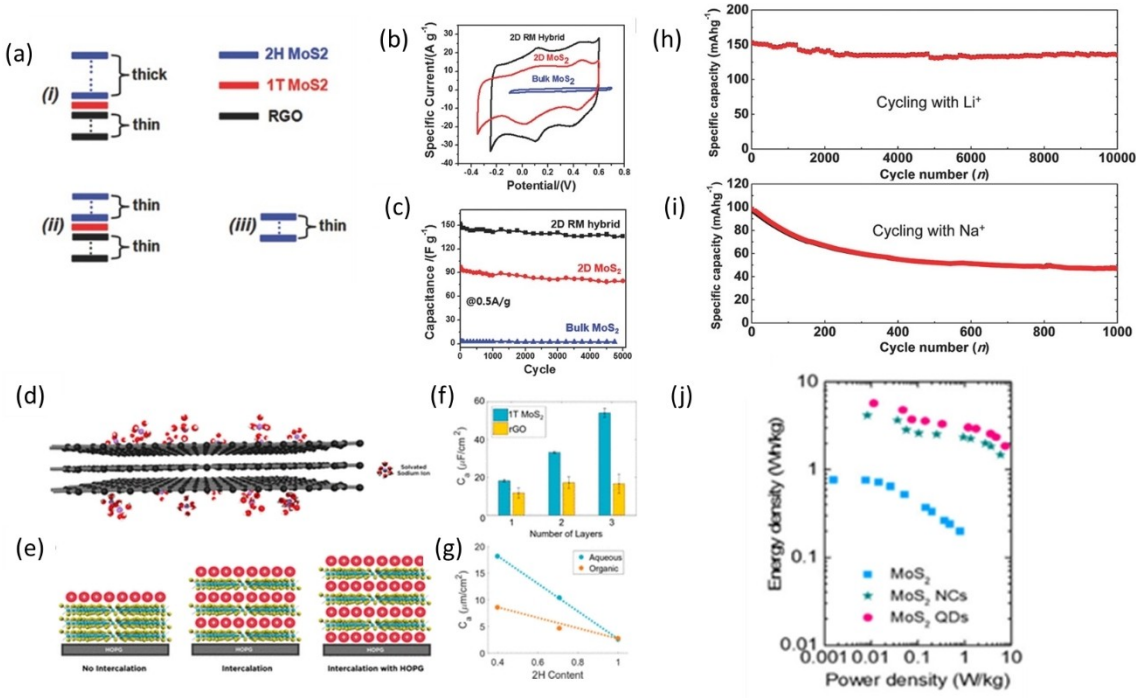

Figure 8. (a) Schematic of 1 T–MoS_2 existing among the RGO and 2 H–MoS_2 heterostructure, electrochemical behavior of (b) CVs, (c) GCD curves of bulk and 2 D MoS_2 in comparison with RGO hybrid heterostructure reproduced with permission[117] copyright © *2015 WILEY-VCH Verlag GmbH & Co. KGaA, Weinheim* (d) An illustration of rGO restack patterns (e) Illustration of different charging methods upon intercalation, no intercalation and intercalation with HDPG (f) Areal capacitance versus layer numbers of 1 T MoS_2, rGO as well as (g) versus 2 H amount reproduced with permission *ACS Nano* **2020**, *14(5)*, 5636–5648 *Copyright © 2020, American Chemical Society*,[116] (h and i) cycling stability of mesoporous–MoS_2 with Na^+, Li^+ intercalation reproduced with permission[103] copyright © *2016 WILEY-VCH Verlag GmbH & Co. KGaA, Weinheim*, (j) Ragone plot of MoS_2 and its derivatives of NCs and QDs Reproduced with permission ACS Omega **2021**, *6(7)*, 4542–4550.[121]

© 2024 The Authors. ChemElectroChem published by Wiley-VCH GmbH

$$MoS_2 + H^+ + e^- = MoS - SH \quad (16)$$

$$MoS_2 + H^+ + e^- = MoS_2 - H \quad (17)$$

At the hybrid interfacial region, the metastable 1 T phase has better stability Figure 8c than the thermodynamically stable 2H phase with RGO contacts.

Cook et al. synthesized mesoporous MoS_2 to explore pseudocapacitive Li^+ and Na^+ ion intercalation, focusing on poor reversibility observed upon intercalation Figure 8h and i.[103] Li^+ intercalation achieved 140 mAh/g within 20 s and retained the capacity over 10,000 consecutive cycles. In 2020, Chen et al. examined the double–layer charge storages mechanism in electrode/electrolyte interfaces based on potential–dependent as well as frequency–dependent behaviors in organic and aqueous electrolytes Figure 8d and e. This was compared with the electrochemical behavior of MoS_2 and RGO layers Figure 8f. The 1 T-phase exhibited a capacitance value of 14.9 μF/cm^2, which is 10 times higher than the 2 H-phase (1.35 μF/cm^2) in an aqueous electrolyte Figure 8g. At higher frequency ranges, the 1 T phase intercalated ions very rapidly due to its layered structure, increasing the energy density values of MoS_2.[116] Basant et al. studied cationic intercalation and its capacitance effects under various electrolytes using MoS_2 with its various polymorphs. Based on the polymorphs of MoS_2 (1 T, 2 H, and 3 R), the surface area of the synthesized MoS_2 varied, impacting the electrochemical performances.[122] Panchu et al. synthesized luminescent quantum dots (~2 nm in size) and nanocrystals derived from 2 D MoS_2 using laser-assisted chemical vapor deposition, showing an extended operation voltage window (0.9 V) with a specific capacitance of 255 F/g. The potentially available active sites of 3D confined MoS_2 as quantum dots, provided greater active site density along with ion intercalation at its dangling edge sites, causing a Faradaic mechanism that ensured an enhanced potential window. The supercapacitor device exhibited an energy density value of ~5.7 Wh kg^{-1} with 95% capacitance retention over 10,000 cycles Figure 8j.[121] Bissett et al. prepared a coin cell supercapacitor consisting of MoS_2-graphene nanocomposites using Na_2SO_4. The incorporation of graphene increased the conductivity and altered the morphology of the cell membrane in supercapacitors. Pseudocapacitance intercalation occurred with Na ions owing to the nature of the layered structure, resulting in an 800% increment in cycling performance.[123]

Considering previous reports, we observed the ion intercalation mechanism, which not only changes its phases but also alters the morphology and surface area of the layered MoS_2 structure. MoS_2 demonstrating both capacitance and pseudocapacitance nature owing to their layered nature and diverse oxidation states of Mo atoms. Thus, a charge transition occurs in terms of charge storage from EDLC to pseudocapacitance. Based on the shape of the CV graph from Figure 9d, the MoS_2 redox reaction indicates the accumulation of ions at the EDL tends to become pseudocapacitance. The nature of low electrical conductivity of 2 H–MoS_2 hinders the electrochemical characteristics in SCs electrode applications. Due to the intercalation mechanisms, the layers are expanded and the 2 H–MoS_2 converted into 1 T–MoS_2. The 1 T-phase of MoS_2 offers ~10^5 times higher conductivity. The enhanced conductivity and hydrophilic nature of 1 T–MoS_2 facilitates an efficient and rapid charge transport characteristics resulting in higher capacitance in line with the increased current. However, the instability nature of 1 T–phase hinders its practical applications. A hybrid of 2 H/1 T–MoS_2 as an excellent technique for combining to attain both the stable and highly conducting MoS_2 electrodes for SCs with enhanced electrochemical performances. Thus, the 1 T–MoS_2 significantly improves the electrochemical behavior of SCs electrode by providing higher conductivity values.

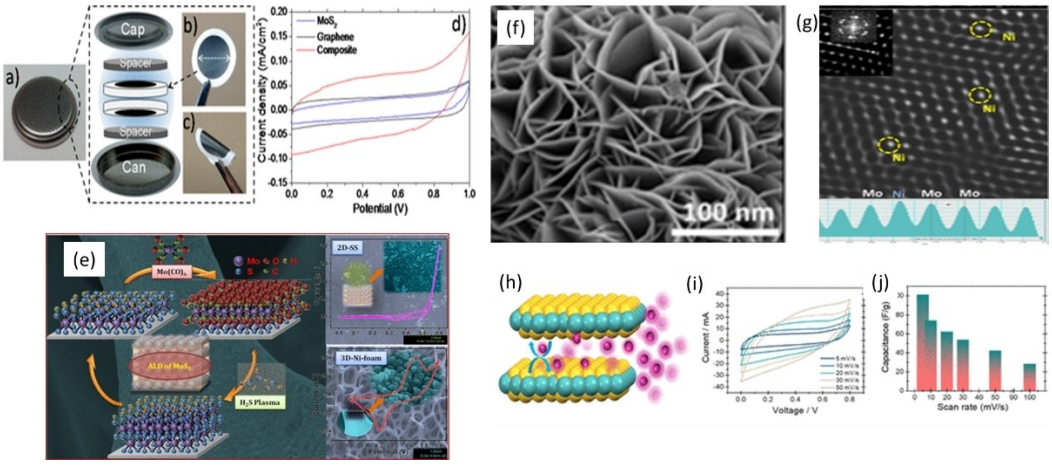

Figure 9. (a) The photo shows the fabricated symmetrical SC coin cell (b, c) images of PVDF membranes fabricated from exfoliated MoS_2 (d) CVs of coin cells fabricated with MoS_2, graphene, and MoS_2–graphene composites using aqueous 1 M Na_2SO_4 adapted with permission from *ACS Appl. Mater. Interfaces* **2015**, *7(31)*, 17388–17398,[123] (e) atomic layer deposition of MoS_2 on stainless steel (SS) and 3D Ni–foam adapted with permission from *ACS Appl. Mater. Interfaces* **2017**, *9(46)*, 40252–40264[124] *Copyright © 2017, American Chemical Society.* (f) morphology of hydrothermally synthesized Ni–MoS_2 flower and (g) its corresponding HRTEM–HAADF images with the inset of SAED pattern, the yellow dots represent the Ni atom dopants (h) schematic representation of ion intercalation mechanism in MoS_2 (i) CVs of Ni–MoS_2 symmetric device containing 1 M Na_2SO_4 aqueous electrolyte and (j) their device capacitance values at various scan rates adapted with permission from *ACS Appl. Energy Mater.* **2023**, *6(4)*, 2187–2198[125] *Copyright © 2023, American Chemical Society.*

© 2024 The Authors. ChemElectroChem published by Wiley-VCH GmbH

The MoS_2/graphene composite, with a 1:3 ratio, demonstrates a substantial areal capacitance (approximately 11 mF/cm^2 at 5 mV/s), prompting the exploration of various 2 D material composites for supercapacitors to improve the performance beyond that of single-component materials in electrochemical energy storage. Nandi et al. employed atomic layer deposition to coat MoS_2 onto stainless–steel (2 D–SS) and three–dimensional (3 D) Nickel foam Figure 9e, serving as electrodes for supercapacitors in both 2 D and 3 D configurations. The 3 D–Ni foam MoS_2 electrodes exhibit behaviors of both EDLC and pseudocapacitance, showcasing the highest areal capacitance value of 3400 mF/cm^2 with 80 % capacitance retention over 4500 cycles.[124] During the electrochemical intercalation/deintercalation process, dopants reduce restacking and improve electrical conductivity. Metal doping has enhanced the internal coulombic efficiency. Thus, dopants in MoS_2 can alter crystal structure, lattice strain, and electrochemical properties towards supercapacitors. Ionic radii play a crucial role when considering doping into MoS_2, and transition metals such as Ni, Co, and Cu are considered more suitable, considerably improving the electrical properties and active sites of MoS_2. Cu-doped MoS_2 reduces resistivity values ten times compared to pristine MoS_2 demonstrated specific capacitance value of 502 F/g in the presence of 1 M Na_2SO_4 electrolyte.[126] Hydrothermally synthesized Cobalt–doped MoS_2 shows 440 F/g in 1 M Na_2SO_4, and its composite with N, S–rGO (Co–MoS_2/N,S–rGO) exhibits an enhanced specific capacitance value (626 F/g) with capacitance retention of 95 % over 4000 cycles.[127] Abraham et al. developed 2D MoS_2 nanosheets derived MoS_2 nanodots infused into Nickel foam, forming a high–performance pseudocapacitance electrode showing a specific capacitance value of 395 F/g in the presence of KOH electrolyte.[128]

A flower–like nickel–doped MoS_2 has been hydrothermally synthesized, where the 2D nanosheets are held together to form a flower–like structure with abundant exposed active edges for ion intercalations, shortening the diffusion length. As depicted in Figure 9f, the Ni–MoS_2 with a highly porous nature provides percolation of electrolyte and higher amounts of ion interaction/diffusion for supercapacitors. Despite high mass loading (~10 mg/cm^2), Ni–MoS_2 morphology enables rapid intercalation/deintercalation (Figure 9h, resulting in high capacitance of ~425 F/g.[125] Redox kinetics and surface reaction rates are significantly affected when the dopant occupies the interstitial position of Mo in MoS_2. Figures 9i and j illustrate the CVs of the Ni–MoS_2 device in 1 M Na_2SO_4 aqueous electrolyte at different voltage sweeps (5 to 50 mV/s), showing a greater current response with a 0–0.8 V voltage window.

4.4. Intercalation Pseudocapacitance in MXenes

Like TMDCs, 2D transition metal carbides, nitrides, and carbonitrides (MXenes) gained popularity as 2D materials in 2011. MXenes are derived from the MAX phase, where M represents transition metals (Ti, Sc, Nb, Mo, Ta, and V), A is from group 13/14 elements, and X is carbon (C) or nitrogen (N). There are 155 discovered MAX phases based on these elemental compositions. The bonding between M–A elements is easily breakable through various synthesis routes, while the M–X bonds are ionic and more challenging to break. The MAX phase has a hexagonal structure with *P_{63}/mmc symmetry*.[129] MXenes are derived from the MAX phase by removing an A atom, forming $Mn+1XnTx$, where Tx represents surface–attached derivatives such as oxygen (O), OH, hydrogen (H), chlorine (Cl), or fluorine (F) ions, and n can be 1, 2, or 3. MXenes are exhibited as M_2X (ABABAB), M_3X_2 (ABCABC), and M_4X_3. When used as electrode materials for supercapacitors, MXenes showcase intercalation of ions as a prominent characteristic of charge storage, with reversible interlayer behavior during charge/discharge. Consequently, MXenes–based supercapacitors exhibit exceptionally high capacitance of 1500 F/cm^3 in aqueous acidic electrolytes. Cation intercalation and surface functional groups (OH^-, F^-, and Cl^-) play a significant role, influencing ion transport and resulting in low energy density values. Theoretical studies provide deeper insights into the structural characteristics of MXenes concerning their adsorbed functional groups, with –O functional groups being highly stable. Generally, both MAX and MXenes are metallic, with their nature varying based on surface–adsorbed functional groups.[130,131] For instance, when Ti_2C relates to –O functional groups, the shift in the d band above the Fermi level (E–Fermi) exhibits semiconducting behavior. Meanwhile, –F adsorbed Ti_2C shows no shift in E–Fermi, displaying metallic behavior.[132] The metallic nature of MXenes (e.g., Ti_3C_2Tx) is highly conductive, providing rapid charge kinetics for supercapacitors.[130,133] The 2D layered structure of MXenes enables the spontaneous intercalation of metal ions (Li^+, Na^+, K^+, NH_4^+, Cs^+, TEA^+, and Mg^{2+}, Ca^{2+}, Al^{3+}), leading to fast charge storage.[134]

The intercalated ions typically reside on the surface adsorptive sites near the edges and in–depth adsorption sites with higher activation energy.[135] In situ XRD analysis revealed that the c–spacing of Ti_3C_2Tx MXene undergoes reversible shrinkage and recovery during electrochemical cycling.[134] The in situ EIS studies on few layered 2 D $Ti_3C_2T_x$ MXene electrodes allow their state of charge and the effects of ions to be tracked. This approach also facilitates the study of the insertion kinetics of various cations. The size of intercalated ions in MXenes directly influences interlayer shrinkage for smaller ionic radii and interlayer expansion for larger ionic radii. Therefore, cationic intercalation and electrostatic interactions within $Ti_3C_2T_x$ result in changes in interlayer distances, expanding if expansion dominates over contraction or contracting if contraction dominates. Deformation behavior of MXene is also influenced by intercalated cations. Xinpeng et al. explored interlayer changes during charge/discharge cycles using H^+ ion intercalation based on a pseudocapacitive mechanism with H_2SO_4 electrolyte. This approach yields higher energy density values than EDLCs due to pseudocapacitance intercalation. Beyond Cs values, the intercalated ions in an aqueous electrolyte have achieved a higher potential–window of −1.2 V for Li_2SO_4 and −0.9 V for H_2SO_4, exhibiting 99.3 % capacitance retention of approximately 10,000 cycles.[137]

Hu et al. conducted in–situ EIS studies on $Ti_3C_2T_x$, as illustrated in Figure 10g and h, introducing various lower

© 2024 The Authors. ChemElectroChem published by Wiley-VCH GmbH

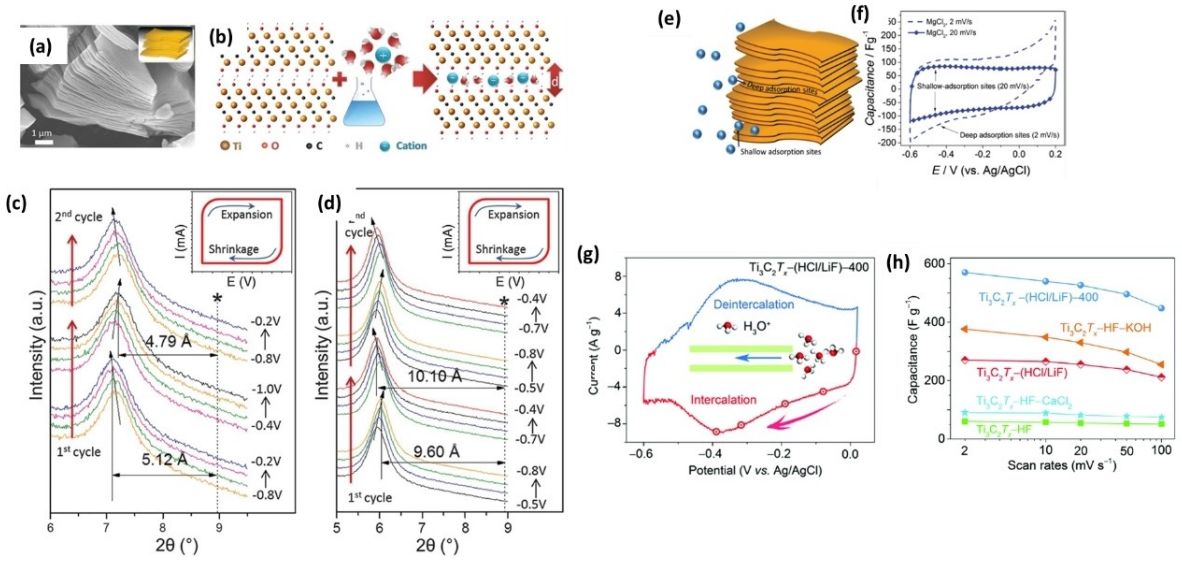

Figure 10. (a) SEM micrographs of $Ti_3C_2T_x$ layers and their schematic representation is given in inset resembling 2D structure, (b) interlayer expansion of MXenes during cation intercalations (c) and (d) *in situ* XRD analysis of $Ti_3C_2T_x$ MXene during charge/discharge process[134] *Copyright © 2013, The American Association for the Advancement of Science* (e) illustration of deep and shallow adsorption sit e (f) Capacitance of $Ti_3C_2T_x$ /carbon black–PTFE in 1 M $MgCl_2$,[135] *© 2014 WILEY-VCH Verlag GmbH & Co. KGaA, Weinheim. In situ electrochemical analysis of* such as CVs of (g) $Ti_3C_2T_x$–(HCl/LiF)–400 (h) gravimetric capacitances measured with varying scanning rates of $Ti_3C_2T_x$ MXenes introduced with different etchants such as HF and HCL/LiF ($Ti_3C_2T_x$–HF and Ti_3C_2Tx–(HCl/LiF), annealing temperature of at 400 °C ($Ti_3C_2T_x$–(HCl/LiF)–400), and KOH as well as $CaCl_2$ treated ($Ti_3C_2T_x$–HF–KOH and $Ti_3C_2T_x$–HF–$CaCl_2$) MXenes[136] reproduced from Ref[136] with permission from the Royal Society of Chemistry.

electronegativity heteroatoms to provide more active sites and rapid charge kinetics. This effort resulted in achieving a capacitance of 570 F/g, and the schematic representation of H^+ ion intercalation/deintercalation is shown in Figure 10g. The gravimetric capacitance measurements for each electrode are compared in the graph in Figure 10h. Notably, $Ti_3C_2T_x$–(HCl/LiF)–400 exhibits significantly higher capacitance than other Ti_3C_2Tx electrodes. Despite the potential to increase capacitance by adjusting interlayer spacing (Figure 11 (a–d)), it is recognized

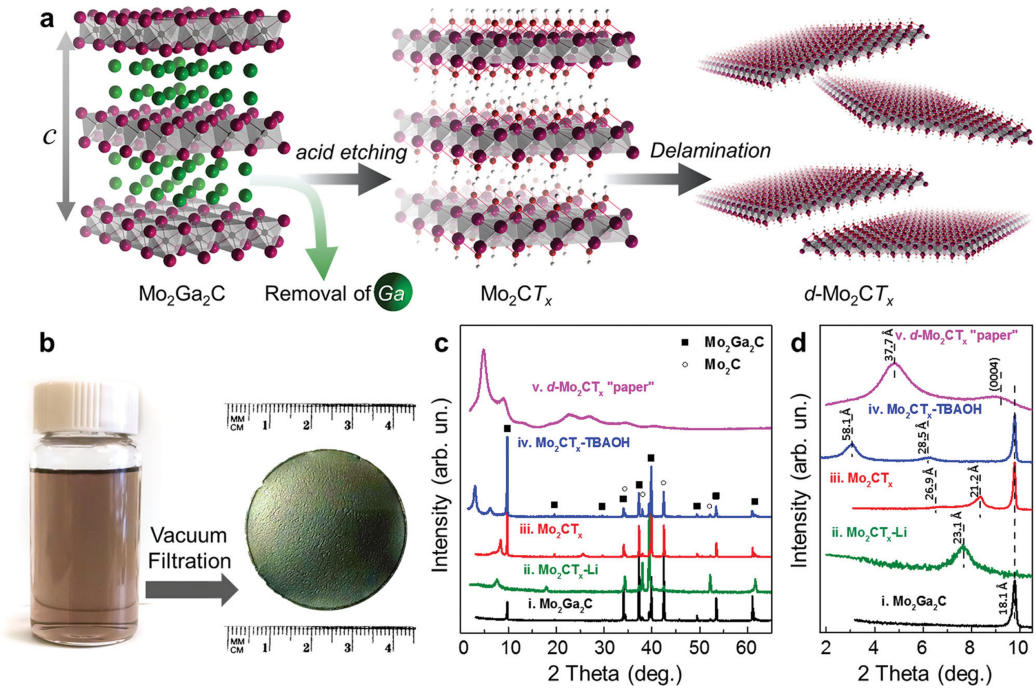

Figure 11. a) Schematic showing preparation of Mo_2CT_x. b) photograph of electrode free paper like material. c) XRD of Mo_2CT_x. d) magnified xrd pattern view (2–10.5°)[138] *© 2016 WILEY-VCH Verlag GmbH & Co. KGaA, Weinheim.*

© 2024 The Authors. ChemElectroChem published by Wiley-VCH GmbH

that this is not the sole factor influencing MXenes' electrochemical performance.[136]

In comparison to carbide–based MXenes, nitride–based MXenes demonstrate excellent intercalation pseudocapacitance. Djire et al. synthesized Ti_2NT_x MXenes as an electrode material for pseudocapacitors in the presence of $MgSO_4$ aqueous electrolyte. Interestingly, the pseudocapacitive mechanism observed in the benchmark Ti_3C_2Tx in H_2SO_4 electrolyte has recently been understood, resulting from the protonation of surface–bound –O groups, leading to changes in Ti atoms' oxidation state at the surfaces.[139] Similarly, Ti_2NT_x MXene might also store charges through a pseudocapacitive mechanism involving changes in Ti oxidation state due to interactions with Mg^{2+} ions.[140] Additionally, non–Ti–MXenes offer various advantages for supercapacitors, such as vanadium carbide (V_4C_3Tx) film displaying prominent pseudocapacitance intercalation mechanisms. The larger interlayer distance of 2.1 nm, while maintaining a layered structure, enhances its features. In its as–fabricated state, the free–standing flexible electrode offers a significant specific capacitance of 292.0 $F g^{-1}$ and excellent electrical conductivity (16,465.3 $S m^{-1}$).[141]

4.5. Intercalation Pseudocapacitance in MoS_2/MXenes Heterostructures

In MoS_2, introducing conductive nanomaterials to create a heterostructure offers an effective approach for enhancing rapid electron transfer and ion diffusion by adjusting interlayer distances. Additionally, MXenes, as 2 D materials, serve as efficient conducting materials and provide a strategy for constructing MoS_2/MXenes heterostructures. The thermodynamic instability of the metallic nature of 1 T MoS_2, which hinders electrochemical performance, has been addressed by establishing stable MoS_2/MXenes heterostructures. Wang et al. developed 1 T–$MoS_2/Ti_3C_2T_x$, where MXenes offer abundant nucleation sites for MoS_2, resulting in the intercalation of more Li^+ ions and rapid ion diffusion, leading to a high capacity of 1160 mAh g^{-1}.[142] Wan et al. synthesized 1 T–MoS_2/Ti_3C_2Tx through a hydrothermal method, exhibiting a high capacitance value of 206.3 $F g^{-1}$ in the presence of 1 M Na_2SO_4 electrolyte, with a retention of 73% Figure 12c. Moreover, Ti_3C_2Tx matrices facilitate rapid electron propagation, while the hybrid structure Figure 12a creates a highly active surface area in the electrolyte, accelerating ion diffusion in their tunnel–like interlayers, as shown in SEM images Figure 12b.[143] The interconnected nature of 3 D 1 T/$Ti_2C_3T_x$ provides more H^+ ions in their heterostructures Figure 12e and f, exhibiting pseudocapacitance contribution due to the intercalation of H^+ ions, with a capacitance value of 386.7 $F g^{-1}$ at 1 $A g^{-1}$ Figure 12d, experiencing only an 8.9% loss after 20000 consecutive cycles in 1 M H_2SO_4.[144] The continuous interaction between MoS_2 and $Ti_2C_3T_x$ prevents aggregation and structural collapse induced by volume changes during the electrochemical charging-discharging process.

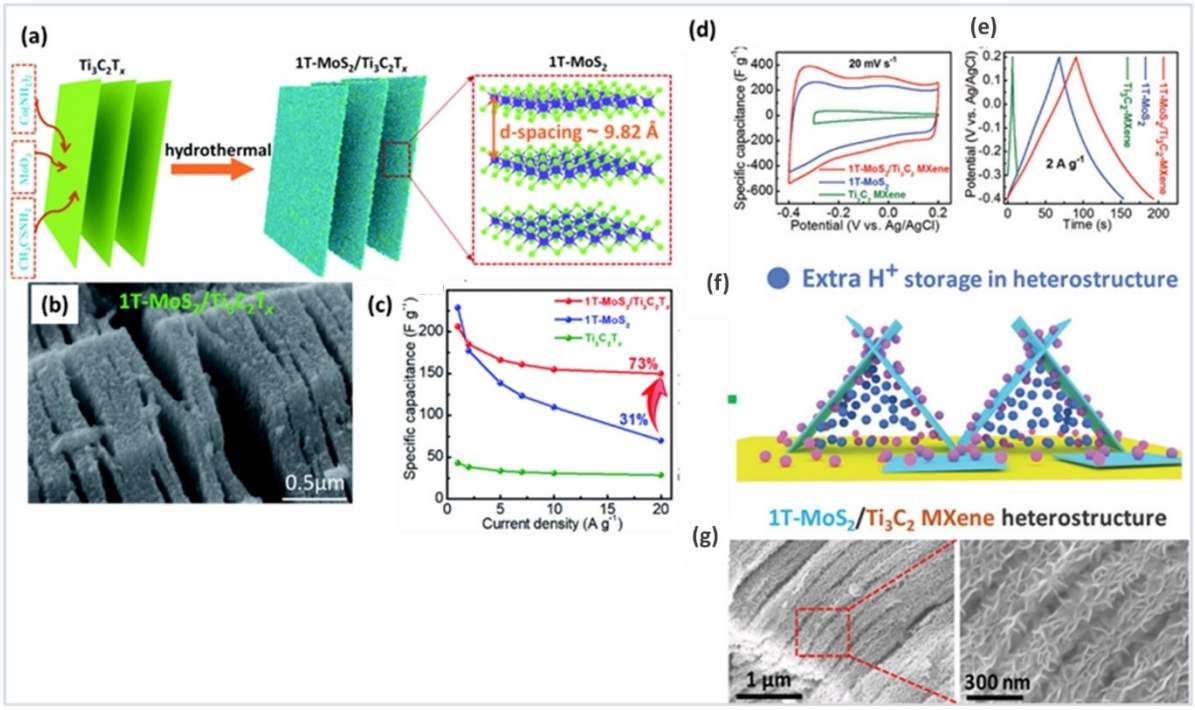

Figure 12. (a) Scheme illustrating the hydrothermally synthesized 1 T–$MoS_2/Ti_3C_2T_x$ heterostructure with d–spacing of 0.982 nm (1 T–MoS_2) (b) Morphology of 1 T–$MoS_2/Ti_3C_2T_x$ obtained from SEM, (c) Gravimetric specific capacitance (vs) Current density of 1 T–MoS_2, $Ti_3C_2T_x$ and 1 T–$MoS_2/Ti_3C_2T_x$[143] Reproduced from Ref.[143] with permission from the Royal Society of Chemistry. (d) CV,(e) GCD curves 1 T–MoS_2, Ti_3C_2 MXene, and 1 T–MoS_2/Ti_3C_2 MXene. f) Schematics of H^+ ions storage the heterostructure during charge/discharge condition. g) SEM micrograph of 1T-MoS_2/Ti_3C_2 electrode as a result of 20000 consecutive cycles[144] Copyright © *2020 WILEY-VCH Verlag GmbH & Co. KGaA, Weinheim.*

© 2024 The Authors. ChemElectroChem published by Wiley-VCH GmbH

4.6. Metal Organic Frameworks

Metal organic frameworks (MOFs) are emerging category of nanoporous crystalline material called as coordination polymers.[145] Among various MOFs, there are 30 types are utilized for SCs application.[146] Among them layered compounds are becoming popular due to their outstanding electrochemical characteristics. MOFs can be widely used as electrode materials for SCs due to their controlled synthesis with porous structures. The porous nature and the metal cations exist in MOFs can accommodate the electrolyte ions and acts as a reactive active site.[147–149] It is possible to design and synthesize new coordination polymers with pseudocapacitive redox metal ions as well as pores/spaces large enough for electrolyte transport and storage. Yang et al. introduced nickel–MOF (Ni–MOF) based on *p*-benzene dicarboxylic acid (PTA) ligand as an electrode material for SCs application and their capacitance value has been achieved 1127 F/g with capacitance retention of 90% over 3000 cycles.[150] The intercalation of OH– ions that has been explained in the below equation (Equation (18))

$$[Ni\ (OH)_2\ (C_8H_4O_4)_2.(H_2O)_4\ ].\ 2H_2O + OH^- - e^- \leftrightarrow [Ni_3\ O(OH)(C_8H_4O_4)_2.(H_2O)_4].\ 2H_2O + \ 2H_2O \quad (18)$$

Yang et al. doped the Ni–MOF with zinc (Zn) and achieved a capacitance values of 1620 F/g with 91% retaining capacitance over 3000 Cycles[151] than previously reported pure Ni–MOF. The OH– ions are intercalated and de–intercalated during redox reactions due to the pseudocapacitive mechanism. In addition to providing enough space for electrolyte diffusion, Ni–MOF facilitates OH^- intercalation and deintercalation owing to their layered nature. Wen et al. utilized Ni–MOF where the organic linker is 1,4-dicarboxybenzene (H_2BDC), with carbon nanotubes composite to achieve increased capacitance values of 1765 F g^{-1} and their capacitance retention was 95% over 5000 cycles. The introduced CNTs are acts as a current collector and lower the charge–transfer resistance values to improve the rapid redox reactions during charge/discharge process.[152] Qu et al. synthesized Ni–MOF using 9,10-anthracenedicarboxylic acid (ADC) and achieved 552 F/g and capacitance retention of >98% after 16,000 cycles. Due to the intercalation/de-intercalation of OH^- during electrochemical reactions, Ni^{2+} and Ni^{3+} valence states can be reversibly changed. After the charge/discharge processes, the precise mechanism of the structure change and the final structure of MOFs is still unclear, and more advanced characterization methods are needed.[153] Liu et al. used hexamethylenetetramine and 2,3,5,6-tetrafluoroterephthalic acid as a ligand source to synthesis Co–MOF, and it demonstrated the pseudocapacitance behaviour with the capacitance value of 2474 F g^{-1} and stable over 2000 cycles.[147] Yang et al. used p-benzene dicarboxylic acid (PTA) as an organic ligand to synthesis Cobalt based MOF (Co–MOF) nanosheets which exhibit with pseudocapacitance intercalation behaviour and demonstrated the specific capacitance value of 2564 F/g and the capacitance retention of 95.8% at 3000 cycles.[154] The layered nature of MOFs facilitates the intercalation/de-intercalation of OH^- species in their layers Figure 13a, also provides a pathway for electron transport Figure 13b the mechanism can be explained by the below equation as (Equation (19) and (20))

$$Co(II)_s + OH^- \leftrightarrow Co(II)_s(OH)_{ad} + e^- \quad (19)$$

$$Co(II)_s(OH)_{ad} \leftrightarrow Co(II)_s(OH)_{ad} \ + e^- \quad (20)$$

Banda et al. studied the Li+ intercalation mechanism in nonporous 2 D coordination polymer, where the nickel metal was coordinate with the benzenehexathiolate (BHT) called as Ni_3BHT which delivered excellent specific capacitance of 245 F/g in presence of lithium hexafluorophosphate ($LiPF_6$)/MeCN electrolytic solution to ensure that cations could intercalate between Ni_3BHT layers. A small cation size results in higher capacitance values. The electrochemical analysis confirming the adsorption of ions on Ni_3BHT results in higher capacitance values.[155]

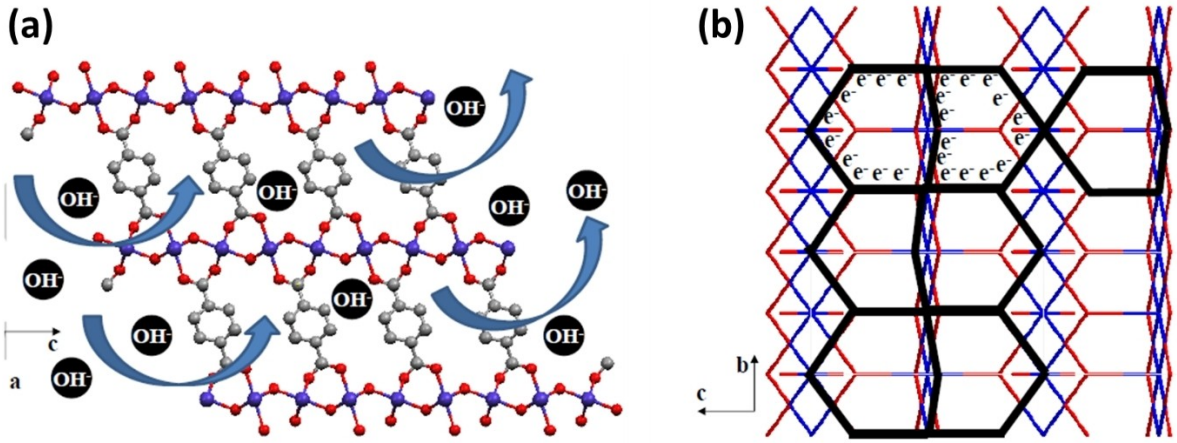

Figure 13. An illustration of (a) Intercalation and deintercalation of OH^- species in the layers of Co–MOF and (b) their e^- transfer in 2 D conductive pathways I[154] *Copyright © 2017 Wiley-VCH Verlag GmbH & Co. KGaA, Weinheim.*

© 2024 The Authors. ChemElectroChem published by Wiley-VCH GmbH

5. Challenges and Opportunities in Intercalation Pseudocapacitance

The utilization of highly porous electrode materials, such as carbon, has demonstrated elevated capacitance values attributed to mechanisms like ion dissolution and non–Coulombic ion ordering. These mechanisms resemble those found in redox–based 2 D layered nanomaterials when interacting with electrolytes. Pseudocapacitance, a concept shared by electrochemical capacitors and intercalation–type batteries, explores charge transfer mechanisms at an electrochemical interface. Unlike Li–ion batteries, which study solid–state processes, pseudocapacitance delves into electrochemical and surface chemical reactions for energy storage devices, bridging fundamental electrochemistry and surface science with applications in electrochemical energy storage (EES).[165] The materials discussed in this review offer broad applications in various fields of EES devices. This review intends to underscore the potential advantages of pseudocapacitive ion intercalation using 2 D layered materials. The review emphasizes the need to optimize composite electrode architecture for nanostructured pseudocapacitive active materials, particularly by combining 2 D nanomaterials in composite electrodes.[166]

In contrast to carbide–based MXenes, nitride-based MXenes exhibit excellent intercalation pseudocapacitance. Djire et al. synthesized Ti_2NTx MXenes as electrode materials for pseudocapacitors in the presence of $MgSO_4$ aqueous electrolyte. Pseudocapacitive mechanisms, such as protonation of surface–bound –O groups, have been recently understood and play a crucial role in $Ti_3C_2T_x$ in H_2SO_4 electrolyte. Similarly, Ti_2NT_x MXene may store charges via a pseudocapacitive mechanism involving changes in Ti oxidation state due to interactions between Mg^{2+} ions.[140] Furthermore, non–Ti MXenes, such as vanadium carbide ($V_4C_3T_x$), demonstrate prominent pseudocapacitive intercalation mechanisms. The film exhibits a larger interlayer distance of 2.1 nm while maintaining a layered structure, resulting in a significant specific capacitance of 292.0 F/g and excellent electrical conductivity (16,465.3 $S\,m^{-1}$) in its as–fabricated state.[141] The incorporation of conductive nanomaterials to create a heterostructure in MoS_2 facilitates rapid electron transfer and ion diffusion by increasing interlayer distances. MXenes, as 2 D materials, serve as efficient conducting materials and offer a strategy for constructing MoS_2/MXenes heterostructures. The metallic nature of 1 T MoS_2, which is thermodynamically unstable, is addressed by forming stable MoS_2/MXenes. Various studies, such as those by Wang et al.[142] and Wan et al.[143] have demonstrated the enhanced capacity and performance achieved in MoS_2/MXenes heterostructures.

The intercalation in 2 D materials are occurs through two different mechanisms such as, (i) For intercalation, partially dissolved electrolyte species require dissolution, resulting in a negligible impact on d spacing, (ii) the ion intercalation can lead to the exfoliation of electrode materials within the device. If the materials are weak vdW interaction can undergo exfoliation, but it highly depends on the electrode/electrolyte interactions.[167] The layer numbers in 2 D nanosheets are important in intercalation mechanisms, which should be investigated for a variety of pseudocapacitive electrode materials based on chalcogenides. By establishing a fundamental understanding of heterointerfaces and their interactions, a more comprehensive knowledge of the heterostructure and interactions of 2 D hybrid nanosheets such as phase transition as well as intercalation chemistry can be achieved. Based on these observations, we can engineer pseudocapacitive intercalation electrode fabrications using information regarding the intercalation chemistry of graphene, TMOs, MoS_2, MXenes and MOFs and other 2 D materials. Additionally, discovering these pseudocapacitive materials (Table 1) has great importance considering their potential to overcome key issues that SCs are currently facing. These issues include poor cycling stability and low power for EDLC–based devices as well as low capacitance of the devices based on EDLC technology.

In conclusion, this review emphasizes the significance of pseudocapacitive ion intercalation in enhancing energy storage devices using 2 D materials such as graphene, 2 D TMOs, MoS_2, MXenes and 2 D MOFs. The unique properties of these materials, such as large 2 D structures and pseudocapacitive charge storage mechanisms, make them promising candidates for advanced energy storage applications. The ongoing research and development in this field aims to optimize electrode architectures and understand the fundamental intercalation mechanisms for further improvements in energy density and cycling stability.

In–depth analytical approaches are crucial for a comprehensive comprehension of the factors influencing electrochemical features in pseudocapacitance intercalation related to electrode materials. This understanding necessitates a grasp of specific electrode design aspects, encompassing composition and structure.[168] To explore and optimize the performance of pseudocapacitive electrode materials, density functional theory and computational studies at the nano and atomic levels are imperative. These studies elucidate energy level interactions involving ionic and valence electrons.[169] Enhanced electrode performance necessitates a detailed understanding of material interactions, structures, morphologies, and electrochemical functionality, achievable through in–situ or ex–situ analyses.[170] To delve into the fundamental mechanisms of charge–discharge reactions, thorough calculations and simulations are strongly recommended. Efficient synthetic strategies, such as the formation of heterostructures, induction of phase transitions, incorporation of various transition metal dopants, development of nanocomposites with conducting materials, and the design of high mass loading electrodes, are essential for the rational design and fabrication of electrode materials.

6. Conclusions

In conclusion, the development of superior electrode materials with enhanced electrochemical performance requires precise design, synthesis strategies, and nanostructure engineering. Addressing concerns related to unsuitable compositions, geometries, and shapes of pseudocapacitive materials can be achieved by improving existing procedures and developing novel methods for composite material production. The functional design of electrode materials, focusing on controlling physiochemical properties such as crystal structure, atomic arrangement, defects, and multivalence of metallic sites, can significantly enhance the electrochemical performance of

© 2024 The Authors. ChemElectroChem published by Wiley-VCH GmbH

Table 1. Comparison of SCs behaviour of MoS_2, transition metal doped MoS_2, MoS_2 composite with carbon heterostructure, MXenes an MoS_2/MXenes heterostructure in various electrolytes.

Material	Morphology	Capacitance	Electrolyte	Reference
MoS_2	Nano Walls	100 F g^{-1}	H_2SO_4	104
MoS_2	Free standing Nanosheets	8 mF cm^{-2}	KOH	156
MoS_2	Sphere	92.85 F g^{-1}	1 M Na_2SO_4	157
MoS_2	Nano Sphere	122 F g^{-1}	1 M KCl	158
MoS_2	Mesoporous	403 F g^{-1}	1 M Na_2SO_4	159
MoS_2	Nanodots	395 F g^{-1}	KOH	128.
Cu–MoS_2		502 F g^{-1}	1 M Na_2SO_4	126
Co–MoS_2		440 F/g	1 M Na_2SO_4	127
Co–MoS_2/N,S–rGO		626 F g^{-1}		
$Ti_3C_2T_x$	Compact film	245 F g^{-1}	1 M H_2SO_4/Aqueous	160
$Ti_3C_2T_x$	Vertically aligned	270 F g^{-1}	1 M H_2SO_4/Aqueous	161
$Mo_{1.33}CT_x$	Paper electrode	339 F g^{-1}	1 M H_2SO_4/Aqueous	162
Mo_2CT_x	Paper electrode	700 F cm^{-3}	1 M H_2SO_4/Aqueous	138
$Ti_3C_2T_x$		570 F g^{-1}	1 M H_2SO_4	136
$Ti_3C_2T_x$	hydrogel film	70 F g^{-1}	EMI–TFSI (Non Aqueous)	163
Ti_2NT_x	nanosheets	$>$200 F g^{-1}	1 M $MgSO_4$ Aqueous	140
$Ti_3C_2T_x$	Hydrogel	226 F g^{-1}	3 M H_2SO_4/Aqueous	164
$V_4C_3T_x$	free–standing flexible electrode	292.0 F g^{-1}	–	141

SCs. Integrating less conducting 2 D materials with highly conducting counterparts to form heterostructures, capable of pseudocapacitance intercalation, holds promise for improving electrode materials' electrochemical performances. From the review perspective, remarkable progress has been made in 2 D materials–based electrodes for SCs. Various nanostructures of MoS_2, maintaining the layered nature while introducing different configurations, have demonstrated pseudocapacitance intercalation, leading to higher energy density values. Combining MoS_2 with graphene or carbon-based materials enhances conductivity, reducing irreversible processes during charging/discharging cycles. This overview emphasizes the potential of emergence 2 D materials such as MoS_2, MXenes, and 2 D MOFs as supercapacitor materials for electrochemical applications. The investigation of defects, dopants, and nanocomposites highlights their impact on electronic and structural characteristics in the context of the pseudocapacitance intercalation mechanism. The pseudocapacitance mechanism's efficacy depends on amount of surface–active sites at the electrode/electrolyte interface. An in–depth analysis of in situ studies in order to comprehend the electrochemical behaviour during the charging/discharging contribute to the future advancements of energy storage devices.

Acknowledgements

The authors gratefully acknowledge the financial support from the South African Research Chairs Initiative (SARChI) of the Department of Science and Technology and the National Research Foundation of South Africa (84415).

Conflict of Interests

The authors declare no conflict of interest.

Keywords: Intercalation pseudocapacitance · TMDCs · MXenes · Supercapacitors · MOFs

[1] L. Zhang, X. S. Zhao, *Chem. Soc. Rev.* **2009**, *38*, 2520–2531.
[2] A. Noori, M. F. El-Kady, M. S. Rahmanifar, R. B. Kaner, M. F. Mousavi, *Chem. Soc. Rev.* **2019**, *48*, 1272–1341.
[3] J. B. Goodenough, *Acc. Chem. Res.* **2013**, *46*, 1053–1061.
[4] M. Tomy, A. Ambika Rajappan, V. Vm, X. Thankappan Suryabai, *Energy Fuels* **2021**, *35*, 19881–19900.
[5] P. Simon, Y. Gogotsi, *Nat. Mater.* **2020**, *19*, 1151–1163.
[6] M. Winter, R. J. Brodd, *Chem. Rev.* **2004**, *104*, 4245–4270.
[7] P. Simon, Y. Gogotsi, *Nat. Mater.* **2008**, *7*, 845–854.
[8] Allen J. Bard, G. Inzelt, S. Fritz, *Electrochemical Dictionary* Springer Berlin Heidelberg, Berlin, Heidelberg, **2012**, 1–991.
[9] V. Augustyn, P. Simon, B. Dunn, *Energy Environ. Sci.* **2014**, *7*, 1597–1614.
[10] Z. Lei, X. Sun, H. Wang, Z. Liu, X. S. Zhao, *ACS Appl. Mater. Interfaces* **2013**, *5*, 7501–7508.
[11] P. Nakhanivej, Q. Dou, P. Xiong, H. S. Park, *Acc Mater Res.* **2021**, *2*, 86–96.
[12] P. Forouzandeh, S. C. Pillai, *Mater. Today: Proc.* **2021**, *41*, 498–505.
[13] J. N. Coleman, M. Lotya, A. O'Neill, S. D. Bergin, P. J. King, U. Khan, K. Young, A. Gaucher, S. De, R. J. Smith, I. V. Shvets, S. K. Arora, G. Stanton, H. Y. Kim, K. Lee, G. T. Kim, G. S. Duesberg, T. Hallam, J. J. Boland, J. J. Wang, J. F. Donegan, J. C. Grunlan, G. Moriarty, A. Shmeliov, R. J. Nicholls, J. M. Perkins, E. M. Grieveson, K. Theuwissen, D. W. McComb, P. D. Nellist, V. Nicolosi, *Science* **2011**, *331*, 568–571.
[14] J. Yan, Q. Wang, T. Wei, Z. Fan, *Adv. Energy Mater.* **2014**, *4*, 1300816.
[15] Z. Zhang, X. Liu, J. Yu, Y. Hang, Y. Li, Y. Guo, Y. Xu, X. Sun, J. Zhou, W. Guo, *Wiley Interdiscip. Rev. Comput. Mol. Sci.* **2016**, *6*, 324–350.
[16] Q. Tang, Z. Zhou, Z. Chen, *J. Phys. Chem. C.* **2011**, *115*, 18531–18537.
[17] M. J. Allen, V. C. Tung, R. B. Kaner, *Chem. Rev.* **2010**, *110*, 132–145.

© 2024 The Authors. ChemElectroChem published by Wiley-VCH GmbH

[18] Q. Tang, Y. Cui, Y. Li, Z. Zhou, Z. Chen, *J. Phys. Chem. C.* **2011**, *115*, 1724–1731.
[19] T. Gu, W. Luo, H. Xiang, *Wiley Interdiscip. Rev.: Comput. Mol. Sci.* **2017**, *7*, 1–18.
[20] T. Xia, Y. Wang, C. Mai, G. Pan, L. Zhang, W. Zhao, J. Zhang, *RSC Adv.* **2019**, *9*, 19253–19260.
[21] T. Zhai, H. Liu, H. Li, X. Fang, M. Liao, L. Li, H. Zhou, Y. Koide, Y. Bando, D. Golberg, *Adv. Mater.* **2010**, *22*, 2547–2552.
[22] J. Fei, L. Meng, T. Nie, Y. Luan, *Phys Status Solidi B Basic Res.* **2017**, *254*, 1600728.
[23] H. Wang, D. Yang, J. Yang, X. Ma, H. Li, W. Dong, R. Zhang, C. Feng, *ChemCatChem.* **2021**, *13*, 2570–2576.
[24] K. S. Kumar, N. Choudhary, Y. Jung, J. Thomas, *ACS Energy Lett.* **2018**, *3*, 482–495.
[25] D. Yuan, Y. Dou, Y. Tian, D. Adekoya, L. Xu, S. Zhang, *Angew. Chem.* **2021**, *60*, 18830–18837.
[26] T. Purkait, G. Singh, M. Singh, D. Kumar, R. S. Dey, *Sci. Rep.* **2017**, *7*, 15239.
[27] M. J. Molaei, M. Younas, M. Rezakazemi, *ACS Appl. Electron. Mater.* **2021**, *3*, 5165–5187.
[28] J. Cherusseri, N. Choudhary, K. Sambath Kumar, Y. Jung, J. Thomas, *Nanoscale Horiz.* **2019**, *4*, 840–858.
[29] H. D. Yoo, Y. Li, Y. Liang, Y. Lan, F. Wang, Y. Yao, *ChemNanoMat.* **2016**, *2*, 688–691.
[30] L. Fu, W. Xia, *Adv. Eng. Mater.* **2021**, *23*, 2001191.
[31] X. Xu, J. Yang, Y. Hong, J. Wang, *ACS Appl. Nano Mater.* **2022**, *5*, 8382–8392.
[32] M. Ojha, B. Wu, M. Deepa, *ACS Appl Mater Interf.* **2020**, *12*, 42749–42762.
[33] X. Y. Hou, X. L. Yan, X. Wang, S. Li, Y. Jiang, M. Hu, Q. G. Zhai, *Cryst. Growth Des.* **2018**, *18*, 6035–6045.
[34] M. Acerce, D. Voiry, M. Chhowalla, *Nat. Nanotechnol.* **2015**, *10*, 313–318.
[35] A. Bhat, S. Anwer, K. S. Bhat, M. I. H. Mohideen, K. Liao, A. Qurashi, *NPJ 2D Mater. Appl.* **2021**, *5*, 61.
[36] C. Meng, P. Das, X. Shi, Q. Fu, K. Müllen, Z. S. Wu, *Small Science* **2021**, *1*, 2000076.
[37] Y. Shao, M. F. El-Kady, J. Sun, Y. Li, Q. Zhang, M. Zhu, H. Wang, B. Dunn, R. B. Kaner, *Chem. Rev.* **2018**, *118*, 9233–9280.
[38] L. Zhang, X. S. Zhao, *Chem. Soc. Rev.* **2009**, *38*, 2520–2531.
[39] J. M. Lim, Y. S. Jang, H. Van T Nguyen, J. S. Kim, Y. Yoon, B. J. Park, D. H. Seo, K. K. Lee, Z. Han, K. Ostrikov, S. G. Doo, *Nanoscale Adv.* **2023**, *5*, 615–626.
[40] R. Kö Tz, M. Carlen, *Electrochim. Acta* **2000**, *45*, 2483–2498.
[41] Y. Zhai, Y. Dou, D. Zhao, P. F. Fulvio, R. T. Mayes, S. Dai, *Adv. Mater.* **2011**, *23*, 4828–4850.
[42] D. C. Grahame, *J. Am. Chem. Soc.* **1941**, *63*, 1207–1215.
[43] B. E. Conway, E. Gileadi, *Trans. Faraday Soc.* **1962**, *58*, 2493–2509.
[44] S. Srinivasan, E. Gileadi, *Electrochim. Acta* **1966**, *11*, 321–335.
[45] T. Brousse, D. Bélanger, J. W. Long, *J. Electrochem. Soc.* **2015**, *162*, A5185–A5189.
[46] H. Huang, M. Niederberger, *Nanoscale* **2019**, *11*, 19225–19240.
[47] B. Y. Chang, E. Ahn, S. M. Park, *J. Phys. Chem. C* **2008**, *112*, 16902–16909.
[48] D. Rochefort, A. L. Pont, *Electrochem. Commun.* **2006**, *8*, 1539–1543.
[49] S. Trasatti, G. Buzzanca, *J. Electroanal. Chem. Interf. Electrochem* **1971**, *29*, A1–A5.
[50] V. Augustyn, J. Come, M. A. Lowe, J. W. Kim, P. L. Taberna, S. H. Tolbert, H. D. Abruña, P. Simon, B. Dunn, *Nat. Mater.* **2013**, *12*, 518–522.
[51] V. Augustyn, J. Come, M. A. Lowe, J. W. Kim, P. L. Taberna, S. H. Tolbert, H. D. Abruña, P. Simon, B. Dunn, *Nat. Mater.* **2013**, *12*, 518–522.
[52] Y. Jiang, J. Liu, *Energy Environ. Mater.* **2019**, *2*, 30–37.
[53] V. Augustyn, J. Come, M. A. Lowe, J. W. Kim, P. L. Taberna, S. H. Tolbert, H. D. Abruña, P. Simon, B. Dunn, *Nat. Mater.* **2013**, *12*, 518–522.
[54] J. Wang, J. Polleux, J. Lim, B. Dunn, *J. Phys. Chem. C* **2007**, *111*, 14925–14931.
[55] J. M. Tarascon, M. Armand, *Nature* **2001**, *414*, 359–367.
[56] A. Patil, V. Patil, D. Wook Shin, J. W. Choi, D. S. Paik, S. J. Yoon, *Mater. Res. Bull.* **2008**, *43*, 1913–1942.
[57] C. Sassoye, C. Laberty, H. Le Khanh, S. Cassaignon, C. Boissière, M. Antonietti, C. Sanchez, *Adv. Funct. Mater.* **2009**, *19*, 1922–1929.
[58] K. Brezesinski, J. Wang, J. Haetge, C. Reitz, S. O. Steinmueller, S. H. Tolbert, B. M. Smarsly, B. Dunn, T. Brezesinski, *J. Am. Chem. Soc.* **2010**, *132*, 6982–6990.
[59] J. W. Kim, V. Augustyn, B. Dunn, *Adv. Energy Mater.* **2012**, *2*, 141–148.
[60] T. Brezesinski, J. Wang, S. H. Tolbert, B. Dunn, *Nat. Mater.* **2010**, *9*, 146–151.
[61] T. Ling, P. Da, X. Zheng, B. Ge, Z. Hu, M. Wu, X.-W. Du, W.-B. Hu, M. Jaroniec, S.-Z. Qiao, *Sci. Adv.* **2018**, *4*, 1–8.
[62] X. Yu, S. Yun, J. S. Yeon, P. Bhattacharya, L. Wang, S. W. Lee, X. Hu, H. S. Park, *Adv. Energy Mater.* **2018**, *8*, 1702930.
[63] A. K. Geim, K. S. Novoselov, *Nat. Mater.* **2007**, *6*, 183–191.
[64] C. Tan, X. Cao, X. J. Wu, Q. He, J. Yang, X. Zhang, J. Chen, W. Zhao, S. Han, G. H. Nam, M. Sindoro, H. Zhang, *Chem. Rev.* **2017**, *117*, 6225–6331.
[65] Y. Wang, Y. Song, Y. Xia, *Chem. Soc. Rev.* **2016**, *45*, 5925–5950.
[66] T. Kim, S. Lim, K. Kwon, S.-H. Hong, W. Qiao, C. K. Rhee, S.-H. Yoon, I. Mochida, *Langmuir* **2006**, *22*, 9086–9088.
[67] M. D. Stoller, C. W. Magnuson, Y. Zhu, S. Murali, J. W. Suk, R. Piner, R. S. Ruoff, *Energy Environ. Sci.* **2011**, *4*, 4685.
[68] W. Song, X. Ji, W. Deng, Q. Chen, C. Shen, C. E. Banks, *Phys. Chem. Chem. Phys.* **2013**, *15*, 4799.
[69] L. Buglione, E. L. K. Chng, A. Ambrosi, Z. Sofer, M. Pumera, *Electrochem. Commun.* **2012**, *14*, 5–8.
[70] A. Ambrosi, C. K. Chua, N. M. Latiff, A. H. Loo, C. H. A. Wong, A. Y. S. Eng, A. Bonanni, M. Pumera, *Chem. Soc. Rev.* **2016**, *45*, 2458–2493.
[71] L. A. L. Tang, W. C. Lee, H. Shi, E. Y. L. Wong, A. Sadovoy, S. Gorelik, J. Hobley, C. T. Lim, K. P. Loh, *Small* **2012**, *8*, 423–431.
[72] M. D. Stoller, S. Park, Y. Zhu, J. An, R. S. Ruoff, *Nano Lett.* **2008**, *8*, 3498–3502.
[73] D. A. C. Brownson, C. E. Banks, *Chem. Commun.* **2012**, *48*, 1425–1427.
[74] Z. Li, J. Lin, B. Li, C. Yu, H. Wang, Q. Li, *J. Energy Storage* **2021**, *44*, 103437.
[75] M. B. Arvas, H. Gürsu, M. Gencten, Y. Sahin, *J. Energy Storage* **2021**, *35*, 102328.
[76] K. Zhang, L. Mao, L. L. Zhang, H. S. On Chan, X. S. Zhao, J. Wu, *J. Mater. Chem.* **2011**, *21*, 7302.
[77] L. Mao, K. Zhang, H. S. On Chan, J. Wu, *J. Mater. Chem.* **2012**, *22*, 80–85.
[78] L. S. Panchakarla, K. S. Subrahmanyam, S. K. Saha, A. Govindaraj, H. R. Krishnamurthy, U. V. Waghmare, C. N. R. Rao, *Adv. Mater.* **2009**, *21*, 4726–4730.
[79] G. Valtolina, A. Burchianti, A. Amico, E. Neri, K. Xhani, J. A. Seman, A. Trombettoni, A. Smerzi, M. Zaccanti, M. Inguscio, G. Roati, *Science* **2015**, *350*, 1505–1508.
[80] L. S. Panchakarla, K. S. Subrahmanyam, S. K. Saha, A. Govindaraj, H. R. Krishnamurthy, U. V. Waghmare, C. N. R. Rao, *Adv. Mater.* **2009**, *21*, 4726–4730.
[81] D. Wang, F. Li, L. Yin, X. Lu, Z. Chen, I. R. Gentle, G. Q. (Max) Lu, H. Cheng, *Chem. Eur. J.* **2012**, *18*, 5345–5351.
[82] T. Wang, L. X. Wang, D. L. Wu, W. Xia, D. Z. Jia, *Sci. Rep.* **2015**, *5*, 9591.
[83] N. Parveen, M. O. Ansari, S. A. Ansari, M. H. Cho, *J Mater Chem A Mater* **2016**, *4*, 233–240.
[84] G. Arabale, D. Wagh, M. Kulkarni, I. S. Mulla, S. P. Vernekar, K. Vijayamohanan, A. M. Rao, *Chem. Phys. Lett.* **2003**, *376*, 207–213.
[85] C. Xiang, M. Li, M. Zhi, A. Manivannan, N. Wu, *J. Mater. Chem.* **2012**, *22*, 19161.
[86] H. Kim, M. Cho, M. Kim, K. Park, H. Gwon, Y. Lee, K. C. Roh, K. Kang, *Adv. Energy Mater.* **2013**, *3*, 1500–1506.
[87] C. Xiang, M. Li, M. Zhi, A. Manivannan, N. Wu, *J. Power Sources* **2013**, *226*, 65–70.
[88] X. M. Yue, Z. J. Liu, C. C. Xiao, M. Ye, Z. P. Ge, C. Peng, Z. Y. Gu, J. S. Zhu, S. Q. Zhang, *Ionics (Kiel)* **2021**, *27*, 339–349.
[89] A. Soam, R. Kumar, M. C. M. Singh, D. Thatoi, R. O. Dusane, *J. Alloys Compd.* **2020**, *813*, 152145.
[90] Q. Qu, S. Yang, X. Feng, *Adv. Mater.* **2011**, *23*, 5574–5580.
[91] X. Sun, M. Xie, G. Wang, H. Sun, A. S. Cavanagh, J. J. Travis, S. M. George, J. Lian, *J. Electrochem. Soc.* **2012**, *159*, A364–A369.
[92] J. Yan, T. Wei, B. Shao, Z. Fan, W. Qian, M. Zhang, F. Wei, *Carbon N Y* **2010**, *48*, 487–493.
[93] Q. Wu, Y. Xu, Z. Yao, A. Liu, G. Shi, *ACS Nano* **2010**, *4*, 1963–1970.
[94] M. Guan, Q. Wang, X. Zhang, J. Bao, X. Gong, Y. Liu, *Front. Chem.* **2020**, *8*, 1–14.
[95] A. A. Lubimtsev, P. R. C. Kent, B. G. Sumpter, P. Ganesh, *J Mater Chem A Mater* **2013**, *1*, 14951.
[96] H. Liu, Y. Wang, H. Li, W. Yang, H. Zhou, *ChemPhysChem.* **2010**, *11*, 3273–3280.
[97] T. Brezesinski, J. Wang, S. H. Tolbert, B. Dunn, *Nat. Mater.* **2010**, *9*, 146–151.
[98] Q. L. Lu, S. X. Zhao, C. K. Chen, X. Wang, Y. F. Deng, C. W. Nan, *J Mater Chem A Mater* **2016**, *4*, 14560–14566.

© 2024 The Authors. ChemElectroChem published by Wiley-VCH GmbH

[99] H. Pang, Y. Ma, G. Li, J. Chen, J. Zhang, H. Zheng, W. Du, *Dalton Trans.* **2012**, *41*, 13284.
[100] S. J. Panchu, M. K. Moodley, H. C. Swart, *in Handbook on Nanobiomaterials for Therapeutics and Diagnostic Applications* **2021**, Elsevier, 361–384.
[101] B. Zhang, X. Ji, K. Xu, C. Chen, X. Xiong, J. Xiong, Y. Yao, L. Miao, J. Jiang, *Electrochim. Acta* **2016**, *217*, 1–8.
[102] G. A. Muller, J. B. Cook, H. S. Kim, S. H. Tolbert, B. Dunn, *Nano Lett.* **2015**, *15*, 1911–1917.
[103] J. B. Cook, H. S. Kim, Y. Yan, J. S. Ko, S. Robbennolt, B. Dunn, S. H. Tolbert, *Adv. Energy Mater.* **2023**, *6*, 99–108.
[104] J. M. Soon, K. P. Loh, *Electrochem. Solid-State Lett.* **2007**, *10*, 250–254.
[105] J. B. Cook, J. S. Ko, T. C. Lin, D. D. Robertson, H. S. Kim, Y. Yan, Y. Yao, B. S. Dunn, S. H. Tolbert, *ACS Appl Energy Mater* **2023**, *6*, 99–108.
[106] F. Wypych, R. Schöllhorn, *J. Chem. Soc. Chem. Commun.* **1992**, *19*, 1386–1388.
[107] M. A. Py, R. R. Haering, *Can. J. Phys.* **1982**, *61*, 76–84.
[108] L. F. Mattheiss, *Phys. Rev. B.* **1973**, *8*, 3719.
[109] Y. C. Lin, D. O. Dumcenco, Y. S. Huang, K. Suenaga, *Nat. Nanotechnol.* **2014**, *9*, 391–396.
[110] E. Benavente, M. A. Santa Ana, F. Mendizábal, G. González, *Coord. Chem. Rev.* **2002**, *224*, 87–109.
[111] Y. Li, D. Wu, Z. Zhou, C. R. Cabrera, Z. Chen, *J. Phys. Chem. Lett.* **2012**, *3*, 2221–2227.
[112] P. J. Mulhern, *Can. J. Phys.* **1989**, *67*, 1049–1052.
[113] X. Wang, X. Shen, Z. Wang, R. Yu, L. Chen, *ACS Nano* **2014**, *8*, 11394–11400.
[114] R. Wang, S. Wang, X. Peng, Y. Zhang, D. Jin, P. K. Chu, L. Zhang, *Appl Mater Inter* **2017**, *9*, 32745–32755.
[115] T. N. Y. Khawula, K. Raju, P. J. Franklyn, I. Sigalas, K. I. Ozoemena, *J. Mater. Chem. A* **2016**, *4*, 6411–6425.
[116] J. Chen, W. R. Walker, L. Xu, O. Krysiak, Z. She, M. A. Pope, *ACS Nano* **2020**, *14*, 5636–5648.
[117] Q. Mahmood, S. K. Park, K. D. Kwon, S. J. Chang, J. Y. Hong, G. Shen, Y. M. Jung, T. J. Park, S. W. Khang, W. S. Kim, J. Kong, H. S. Park, *Adv. Energy Mater.* **2016**, *6*, 1501115.
[118] R. Shivanna, S. Shoaee, S. Dimitrov, S. K. Kandappa, S. Rajaram, J. R. Durrant, K. S. Narayan, *Energy Environ. Sci.* **2014**, *7*, 435–441.
[119] K. Chang, W. Chen, *ACS Nano* **2011**, *5*, 4720–4728.
[120] G. Gao, W. Gao, E. Cannuccia, J. Taha-Tijerina, L. Balicas, A. Mathkar, T. N. Narayanan, Z. Liu, B. K. Gupta, J. Peng, Y. Yin, A. Rubio, P. M. Ajayan, *Nano Lett.* **2012**, *12*, 3518–3525.
[121] S. J. Panchu, K. Raju, H. C. Swart, B. Chokkalingam, M. Maaza, M. Henini, M. K. Moodley, *ACS Omega* **2021**, *6*, 4542–4550.
[122] B. A. Ali, A. M. A. Omar, A. S. G. Khalil, N. K. Allam, *ACS Appl Mater Inter* **2019**, *11*, 33955–33965.
[123] M. A. Bissett, I. A. Kinloch, R. A. W. Dryfe, *ACS Appl. Mater. Interfaces* **2015**, *7*, 17388–17398.
[124] D. K. Nandi, S. Sahoo, S. Sinha, S. Yeo, H. Kim, R. N. Bulakhe, J. Heo, J. J. Shim, S. H. Kim, *ACS Appl. Mater. Interfaces* **2017**, *9*, 40252–40264.
[125] S. J. Panchu, K. Raju, P. Singh, D. D. Johnson, H. C. Swart, *ACS Appl Energy Mater* **2023**, *6*, 2187–2198.
[126] B. D. Falola, L. Fan, T. Wiltowski, I. I. Suni, *J. Electrochem. Soc.* **2017**, *164*, D674–D679.
[127] S. Silambarasan, T. Maiyalagan, *Mater. Lett.* **2021**, *299*, 130075.
[128] A. M. Abraham, S. P. Lonkar, V. V. Pillai, S. M. Alhassan, *ACS Omega* **2020**, *5*, 11721–11729.
[129] M. Sokol, V. Natu, S. Kota, M. W. Barsoum, *Trends Chem.* **2019**, *1*, 210–223.
[130] J. L. Hart, K. Hantanasirisakul, A. C. Lang, B. Anasori, D. Pinto, Y. Pivak, J. T. van Omme, S. J. May, Y. Gogotsi, M. L. Taheri, *Nat. Commun.* **2019**, *10(522)*, 1–10.
[131] T. Hu, M. Hu, B. Gao, W. Li, X. Wang, *J. Phys. Chem. C* **2018**, *122*, 18501–18509.
[132] L. Li, *Comput. Mater. Sci.* **2016**, *124*, 8–14.
[133] M. Naguib, O. Mashtalir, J. Carle, V. Presser, J. Lu, L. Hultman, Y. Gogotsi, M. W. Barsoum, *ACS Nano* **2012**, *6*, 1322–1331.
[134] M. R. Lukatskaya, O. Mashtalir, C. E. Ren, Y. Dall'Agnese, P. Rozier, P. L. Taberna, M. Naguib, P. Simon, M. W. Barsoum, Y. Gogotsi, *Science* **2013**, *341*, 1502–1505.
[135] M. D. Levi, M. R. Lukatskaya, S. Sigalov, M. Beidaghi, N. Shpigel, L. Daikhin, D. Aurbach, M. W. Barsoum, Y. Gogotsi, *Adv. Energy Mater.* **2015**, *5*, 1400815.
[136] M. Hu, R. Cheng, Z. Li, T. Hu, H. Zhang, C. Shi, J. Yang, C. Cui, C. Zhang, H. Wang, B. Fan, X. Wang, Q. H. Yang, *Nanoscale* **2020**, *12*, 763–771.
[137] J. Li, N. Kurra, M. Seredych, X. Meng, H. Wang, Y. Gogotsi, *Nano Energy* **2019**, *56*, 151–159.
[138] J. Halim, S. Kota, M. R. Lukatskaya, M. Naguib, M. Q. Zhao, E. J. Moon, J. Pitock, J. Nanda, S. J. May, Y. Gogotsi, M. W. Barsoum, *Adv. Funct. Mater.* **2016**, *26*, 3118–3127.
[139] C. Zhan, M. Naguib, M. Lukatskaya, P. R. C. Kent, Y. Gogotsi, D. E. Jiang, *J. Phys. Chem. Lett.* **2018**, *9*, 1223–1228.
[140] A. Djire, A. Bos, J. Liu, H. Zhang, E. M. Miller, N. R. Neale, *ACS Appl. Nano Mater.* **2019**, *2*, 2785–2795.
[141] X. Bin, M. Sheng, Y. Luo, W. Que, *Adv. Mater. Interfaces* **2022**, *9*, 2200231.
[142] L. Wang, X. Zhang, Y. Xu, C. Li, W. Liu, S. Yi, K. Wang, X. Sun, Z. S. Wu, Y. Ma, *Adv. Funct. Mater.* **2021**, *31*, 2104286.
[143] F. Wan, X. Wang, C. Tang, C. Jiang, W. Wang, B. Li, Y. Zhang, X. Zhu, *J Mater Chem A Mater* **2022**, *10*, 12258–12268.
[144] X. Wang, H. Li, H. Li, S. Lin, W. Ding, X. Zhu, Z. Sheng, H. Wang, X. Zhu, Y. Sun, *Adv. Funct. Mater.* **2020**, *30*, 0190302.
[145] K. B. Wang, Q. Xun, Q. Zhang, *EnergyChem* **2020**, *2*, 100025.
[146] J. Yang, Z. Ma, W. Gao, M. Wei, *Chem – Eurn J* **2017**, *23*, 631–636.
[147] X. Liu, C. Shi, C. Zhai, M. Cheng, Q. Liu, G. Wang, *ACS Appl Mater Inter* **2016**, *8*, 4585–4591.
[148] D. Y. Lee, S. J. Yoon, N. K. Shrestha, S.-H. Lee, H. Ahn, S.-H. Han, *Microporous Mesoporous Mater.* **2012**, *153*, 163–165.
[149] R. Díaz, M. G. Orcajo, J. A. Botas, G. Calleja, J. Palma, *Mater. Lett.* **2012**, *68*, 126–128.
[150] J. Yang, P. Xiong, C. Zheng, H. Qiu, M. Wei, *J. Mater. Chem. A* **2014**, *2*, 16640–16644.
[151] J. Yang, C. Zheng, P. Xiong, Y. Li, M. Wei, *J. Mater. Chem. A* **2014**, *2*, 19005–19010.
[152] P. Wen, P. Gong, J. Sun, J. Wang, S. Yang, *J Mater Chem A Mater* **2015**, *3*, 13874–13883.
[153] C. Qu, Y. Jiao, B. Zhao, D. Chen, R. Zou, K. S. Walton, M. Liu, *Nano Energy* **2016**, *26*, 66–73.
[154] J. Yang, Z. Ma, W. Gao, M. Wei, *Chem. Eur. J.* **2017**, *23*, 631–636.
[155] H. Banda, J.-H. Dou, T. Chen, N. J. Libretto, M. Chaudhary, G. M. Bernard, J. T. Miller, V. K. Michaelis, M. Dincă, *J. Am. Chem. Soc.* **2021**, *143*, 2285–2292.
[156] M. Chhowalla, H. S. Shin, G. Eda, L. J. Li, K. P. Loh, H. Zhang, *Nat. Chem.* **2013**, *5*, 263–275.
[157] M. Hakala, R. Kronberg, K. Laasonen, *Sci. Rep.* **2017**, *7*, 15243.
[158] X. Zhou, B. Xu, Z. Lin, D. Shu, L. Ma, *J. Nanosci. Nanotechnol.* **2014**, *14*, 7250–7254.
[159] A. Ramadoss, T. Kim, G. S. Kim, S. J. Kim, *New J. Chem.* **2014**, *38*, 2379–2385.
[160] M. Ghidiu, M. R. Lukatskaya, M. Q. Zhao, Y. Gogotsi, M. W. Barsoum, *Nature* **2015**, *516*, 78–81.
[161] Y. Xia, T. S. Mathis, M. Q. Zhao, B. Anasori, A. Dang, Z. Zhou, H. Cho, Y. Gogotsi, S. Yang, *Nature* **2018**, *557*, 409–412.
[162] B. Ahmed, A. El Ghazaly, J. Rosen, *Adv. Funct. Mater.* **2020**, *30,* 2000894.
[163] Z. Lin, D. Barbara, P. L. Taberna, K. L. Van Aken, B. Anasori, Y. Gogotsi, P. Simon, *J. Power Sources* **2016**, *326*, 575–579.
[164] Y. Deng, T. Shang, Z. Wu, Y. Tao, C. Luo, J. Liang, D. Han, R. Lyu, C. Qi, W. Lv, F. Kang, Q. H. Yang, *Adv. Mater.* **2019**, *31*, 1902432.
[165] S. Fleischmann, J. B. Mitchell, R. Wang, C. Zhan, D. E. Jiang, V. Presser, V. Augustyn, *Chem. Rev.* **2020**, *120*, 6738–6782.
[166] P. Nakhanivej, Q. Dou, P. Xiong, H. S. Park, *Acc Mater Res.* **2021**, *2*, 86–96.
[167] X. Wang, T. S. Mathis, K. Li, Z. Lin, L. Vlcek, T. Torita, N. C. Osti, C. Hatter, P. Urbankowski, A. Sarycheva, M. Tyagi, E. Mamontov, P. Simon, Y. Gogotsi, *Nat. Energy* **2019**, *4*, 241–248.
[168] D. Chen, D. Ding, X. Li, G. H. Waller, X. Xiong, M. A. El-Sayed, M. Liu, *Chem. Mater.* **2015**, *27*, 6608–6619.
[169] D. Chen, J. H. Wang, T. F. Chou, B. Zhao, M. A. El-Sayed, M. Liu, *J. Am. Chem. Soc.* **2017**, *139*, 7071–7081.
[170] C. Meng, P. Das, X. Shi, Q. Fu, K. Müllen, Z. S. Wu, *Small Science* **2021**, *1*, 2000076.

Manuscript received: December 19, 2023
Revised manuscript received: February 29, 2024
Version of record online: ■■, ■■

© 2024 The Authors. ChemElectroChem published by Wiley-VCH GmbH

REVIEW

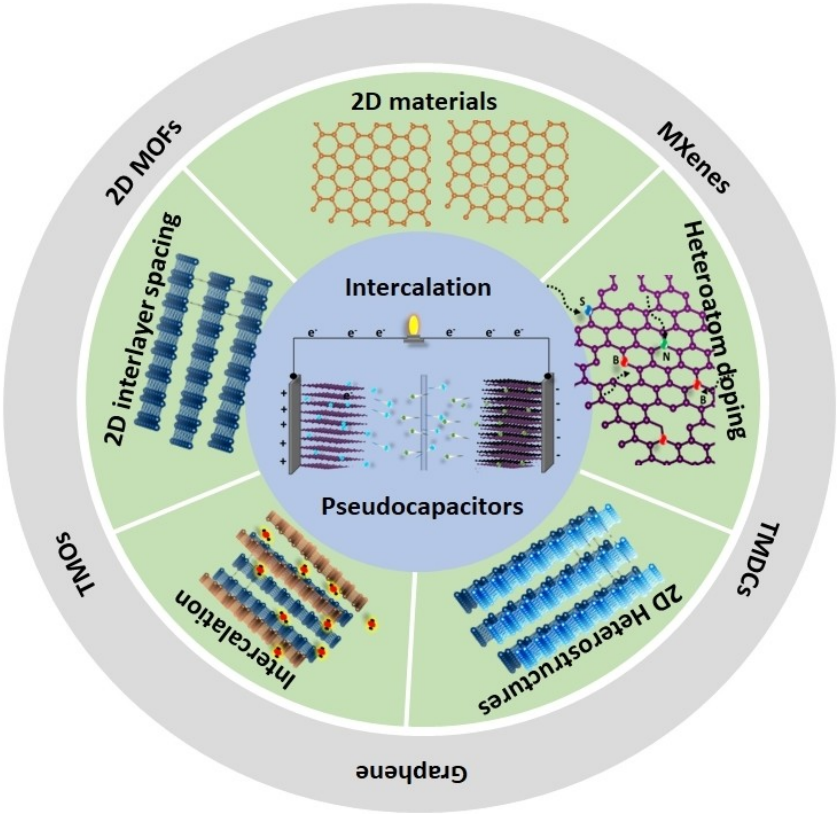

S. J. Panchu, K. Raju, Prof. H. C. Swart**

1 – 23

Emerging Two–Dimensional Intercalation Pseudocapacitive Electrodes for Supercapacitors

Intercalation pseudocapacitive electrodes store energy within the bulk of the electrode via a battery–like intercalation process, effectively bridging the gap between supercapacitors and lithium–ion batteries in terms of energy density and power density. This presents opportunities for further development of 2D materials that offer tunnels or layers for efficient intercalations. Furthermore, there has been progress in enhancing the pseudocapacitance performance of 2D redox–active materials in terms of energy density and cycle stability, to meet the increasing demand for energy storage systems. This review provides a comprehensive analysis of recent advancements in intercalation pseudocapacitors.